A STUDY OF STRUCTURAL DESIGN BASED ON OPTIMALITY

A THESIS SUBMITTED TO
THE GRADUATE SCHOOL OF NATURAL AND APPLIED SCIENCES
OF
MIDDLE EAST TECHNICAL UNIVERSITY

BY

DURUKAN TAMKAN

IN PARTIAL FULFILLMENT OF THE REQUIREMENTS
FOR
THE DEGREE OF MASTER OF SCIENCE
IN
MECHANICAL ENGINEERING

DECEMBER 2019

Approval of the thesis:

A STUDY OF STRUCTURAL DESIGN BASED ON OPTIMALITY

submitted by **DURUKAN TAMKAN** in partial fulfillment of the requirements for the degree of **Master of Science in Mechanical Engineering Department, Middle East Technical University** by,

Prof. Dr. Halil Kalıpçılar
Dean, Graduate School of **Natural and Applied Sciences**   _____

Prof. Dr. M.A. Sahir Arıkan
Head of Department, **Mechanical Engineering**   _____

Prof. Dr. Hakan Işık Tarman
Supervisor, **Mechanical Engineering, METU**   _____

Examining Committee Members:

Prof. Dr. Ender Ciğeroğlu
Mechanical Engineering, METU   _____

Prof. Dr. Hakan Işık Tarman
Mechanical Engineering, METU   _____

Assist. Prof. Dr. Gökhan Özgen
Mechanical Engineering, METU   _____

Assoc. Prof. Dr. Nilay Sezer Uzol
Aerospace Engineering, METU   _____

Assist. Prof. Dr. Onur Baş
Mechanical Engineering, TEDU   _____

Date: 11.12.2019

I hereby declare that all information in this document has been obtained and presented in accordance with academic rules and ethical conduct. I also declare that, as required by these rules and conduct, I have fully cited and referenced all material and results that are not original to this work.

Name, Surname: Durukan Tamkan

Signature:

ABSTRACT

A STUDY OF STRUCTURAL DESIGN BASED ON OPTIMALITY

Tamkan, Durukan
Master of Science, Mechanical Engineering
Supervisor: Prof. Dr. Hakan Işık Tarman

December 2019, 87 pages

Topology optimization is one of the most powerful tool that designers use to reduce weight and cost in aerospace industry. However, traditional manufacturing techniques limits the oncoming advantages of topology optimization.

New manufacturing techniques change the philosophy of topology optimization nearly dismissing the limits of manufacturing. Additive manufacturing not only adjoins complex shapes to design but also adjoins porus/lattice structures.

In the first part of the thesis, a boarding step is optimized with respect to traditional methods with Ti-6Al-4V material and load patterns with respect to stress levels are investigated.

In the second part, the boarding step is optimized with lattice structures without any overall volume reduction with the help of load patterns done in the first part. Optimized lattice design is compared with previous conventional aluminum and 3D woven composite designs

Keywords: Additive manufacturing, Topology optimization, Aircraft structures, Lattice structures, Ti-6Al-4V

ÖZ

YAPISAL TASARIM EN İYİLEŞTİRME ÇALIŞMASI

Tamkan, Durukan
Yüksek Lisans, Makina Mühendisliği
Tez Danışmanı: Prof. Dr. Hakan Işık Tarman

Aralık 2019, 87 sayfa

Topoloji optimizasyonu, tasarımcıların havacılık endüstrisinde ağırlığı ve maliyeti azaltmak için kullandıkları en güçlü araçlardan biridir. Bununla birlikte, geleneksel üretim teknikleri topoloji optimizasyonunun yaklaşmakta olan avantajlarını sınırlamaktadır.

Yeni üretim teknikleri, topoloji optimizasyon felsefesini değiştirmekte; üretim sınırını neredeyse tamamen ortadan kaldırmaktadır. Katmanlı üretim sadece tasarım için karmaşık şekilleri mümkün kılmamış aynı zamanda sünger/hücresel yapılarını da tasarımcıların dünyasına katmıştır.

Tezin ilk bölümünde, Ti-6Al-4V malzeme ile geleneksel yöntemlere göre uçağa biniş/iniş basamağı optimize edilmiş ve stres seviyelerine göre yük yolları incelenmiştir.

İkinci bölümde, biniş/iniş basamağı, birinci bölümde yapılan yük yolları yardımı ile herhangi bir genel hacim azalması olmadan hücresel yapılar ile optimize edilmiştir.

Anahtar Kelimeler: Katmanlı imalat, Topoloji optimizasyonu, Uçak yapıları, hücresel yapılar, Ti-6Al-4V

To my wife Cansu

ACKNOWLEDGEMENTS

I would like to thank my supervisor Prof. Dr. Hakan Işık Tarman for his patience and guidance during the study.

My deep and sincere gratitude to my family for their continuous and unparalleled love, continuous support and for reminding me how lucky I am.

I owe the biggest thanks to Cansu Kuzu Tamkan. I could not succeed without her help, encouragement and love.

I would like to thank my colleagues and my chief in Tusas, Emre Yaban, for their support and understanding in the company during thesis work

TABLE OF CONTENTS

LIST OF TABLES

TABLES

LIST OF FIGURES

FIGURES

LIST OF ABBREVIATIONS

ABBREVIATIONS

FEM	Finite Element Method
IPMS	Infinitely Periodic Minimal Surfaces
Ti	Titanium
AM	Additive Manufacturing
EBM	Electron Beam Melting
SIMP	Solid Isotropic Material with Penalization
RAMP	Rational Approximation of Material Properties
LS	Level Set Approach
GA	Genetic Algorithm
PSO	Particle Swarm Optimization
BESO	Bi-directional evolutionary structural optimization
PLA	Polylactic Acid

LIST OF SYMBOLS

Γ	Lipschitz boundary
Γ_u	Boundary where displacements are prescribed
Γ_t	Boundary where tractions are prescribed
E_e	Stiffness of finite element
E_{ijkl}	Elasticity tensor of order 4
$E_{ijkl}(x)$	Optimal stiffness tensor
E_{ad}	Set of admissible stiffness tensors
E^o_{ijkl}	Stiffness matrix of a given isotropic material
f	Body force
K	Stiffness matrix
K_e	Global level element stiffness matrix
R^n	Metric space, where $n = 2,3$
U	Kinematically admissible displacement fields
t	Boundary tractions on the traction part
$\varnothing$	Arbitrary map
Ω	Large reference domain
Ωmat	Domain occupied by the body

CHAPTER 1

INTRODUCTION

Structural optimization is one of the most trend topics today for weight and cost reduction. There are many methods to provide optimal design but most of them consist of volume reduction. With the additive manufacturing technology, we have the opportunity to create and design porous / low-density structures while keeping the overall volume the same.
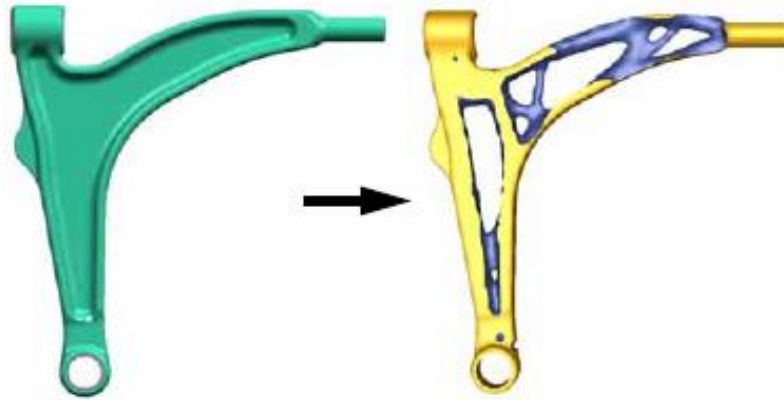
Figure 1.1. Topology Optimization of a Control Arm

As a related topic, lattice structures provide advantages in many respects and they have started to be used in structural designs. While they are most used in medical industry, lattice structures are extending their scope in space and defense industries.

1.1. Thesis Purpose

The main purpose of this study is to optimize an additive manufactured (EBM) aircraft component with lattice structure with respect to weight and stiffness. This study aims to show that additive manufacturing widens the scope of lighter designs without any

functionality lost. The resulting design will be compared with traditionally sized design and 3D woven composite design.

1.2. Definition of Optimal Design

Optimal design of structures has three main components.

(a) *a **model:*** an evaluation of partial differential equation that imitate the properties of mechanical structure.

(b) *an **object function:*** it is also defined as cost function. It is a numerical description of desired case or criteria. It can be maximized or minimized depending on the definition of function.

(c) ***set of constrains***: it is the definition of limitations, optimization variables whom optimal design needs to satisfy.

1.2.1. Parametric or Sizing Optimization

Sizing optimization is the easiest and oldest method to manipulate the problem to reach optimal design. It mainly relies on the optimization of design parameters. In this method a predefined basic structure has to be given beforehand. Each element is determined before optimization and only dimension (i.e. cross section) is allowed to change. Elements does not have the capability to change their position. The success depends on the choice of the basic structure. Numerical values (thickness, length etc.) that effects the object function are taken as values to be optimized.

1.2.2. Shape Optimization

Shape optimization allows the designers to improve design in details with respect to object function without mandatory concept changes. Comparison studies shows that shape and topology optimization has bigger effect on design when compared to sizing techniques [23]. In most of the applications, general effects of design parameters are researched and sensitivity analysis of parameters on design are investigated. [24] In structural applications, it is most commonly done by finite element analysis that

requires boundary/domain corrections to reach reasonable solutions. These problems are overcome by Choi [25], Haslinger and Neittaanmaki [26].

1.2.3. Topology Optimization

First topology optimization was applied nearly 90 years ago by A.G.M Michael [28] the inventor of Michael structures and in the last three decade it is shaped by W.S Hemp [29] and J.M Lagance[30]. Contrary to shape optimization number of elements and their allocations in space are not determined before the optimization. All design space has the potential to be used for final design. Thus it has the capability to shape totally new, unpredictable configurations. Topology optimization is considered as the most advance method in these groups [26]. This methodology and its advantages are even discussed in NATO meetings [27].

1.3. Topology Optimization Methods

The topology optimization concepts widen in all directions with the high desire to build lighter structures. Ancestor of current studies, the homogenization approach, is first published by Bendsøe and Kikuchi in [37]. The method tries to reach the optimal distribution in space of an anisotropic material that is constructed by distributed small holes. [37] It is split into five main fields: "density", "topological derivative", "evolutionary", "level set" and "phase field".

Density and evolutionary topology optimization methods use finite element or point based design variables. Level set optimization method that is combined with topological derivatives in two dimensional problems uses shape derivatives. Moreover, combined approaches such as level set approach that uses shape derivatives without topological derivatives appear in some studies.

1.3.1. Density Methods

Simplified Isotropic Material with Penalization (SIMP) method is introduced just after the homogenization method by Bendsøe [38] in his study "Optimal shape design as a material distribution problem" and it was expanded by Zhou M, Rozvany GIN (1991) [39] and Mlejnek (1992) [40]. SIMP is a simple approach that reduces the complexity of homogenization method. It is also known as power-law approach. The inspiration for the name "power-law approach" comes from the fact that material property is given by a power law. Variations on SIMP have evolved through years and they can be divided into three field approaches:

One-field SIMP: operate only with the design variable field ρ

Two-field SIMP: operate with the design variable field ρ and the physical density field p̄.

Three-field SIMP: operate with the design variable field ρ, the filtered

field p̄ and the projected field

Rational Approximation of Material Properties (RAMP) is an alternative method developed by Stolpe M, Svanberg K (2001) [41]. It is a similar method that only eases the problems that original SIMP interpolation has during convergence to 0-1 solutions. It tries to implement non-zero gradient rather than SIMP but it does not work very well in real life problems.

1.3.2. Topological Derivative Methods

Bubble method is first introduced by Eschenauer in his study "Bubble method for topology and shape optimization of structures."[42] in 1994. The method basically introduces an infinitesimal random hole in the design domain and predicts its derivative and uses this information to create new holes on the design domain.

1.3.3. Evolutionary/Discrete Methods

The original topology optimization problem uses discrete variables and naturally it is expected to be solved by discrete optimization approaches. However, formulation of the problem directly in terms of discrete variables makes the problem very hard to solve. Generally they cannot reach global optimum or be effective for very small problems.

Genetic algorithm is one of the discrete heuristic search methods inspired by Charles Darwin's theory of natural evolution. It is firstly introduced by Holland J. (1970) in his book "Adaptation in Natural and Artificial Systems". Natural selection, crossover and mutation are implemented in binary strings that are created by design parameters like evolution.

Particle swarm optimization is first introduced by Kennedy, J.; Eberhart, R.[45] It is a discrete optimization method that simulates dubbed particles and moves particles in design domain with the help of particle velocity and position.

There are many approaches like genetic algorithms, swarms, ant colony theory algorithms etc. that work surprisingly well for specific problems but general tendency is towards oscillating non convergent endings due to unexpected parameter oscillations.

Bidirectional evolutionary structural optimization (BESO) is like a discrete update version of the standard SIMP method but it does not use power law interpolation parametrization. Lowest strain energy density elements are removed.

1.3.4. Level Set Methods

Level set approach (LS) is a method where boundary is defined by the zero level contour of level set function and the structure is defined by the enclosed domain. Moving boundary is embedded in a scalar function of higher dimension.

Level set methods define the structure shape with the help of solid and void interfaces. It not only allows explicit formulation of objectives /constrains on interface but also is a great tool for stochastic shape variations of robust optimization.

1.3.5. Phase Field Method

Phase field approach directly focus on the density variable and try to minimize the function

$$F(u(\rho),\rho) = \int_{\Omega} \left(\frac{1}{\varepsilon} w(\rho) + \varepsilon \|\nabla\rho\|^2\right) dV + \eta F \qquad (1\text{-}1)$$

where w (ρ) is a function that is zero for both ρ=1 and ρ=0.

The problem with the phase field approach is that update of density field ρ has tendency to divergence. Number of approaches are performed by Bourdin and Chambolle (2003) [43] and Wang and Zhou (2004) [44] with the help of volume constraint but they are not true implementation of phase solutions.

1.3.6. Comparison of topology optimization methods

Most of the work on topology optimization appear to focus on only few of the methods. Most famous one is SIMP, with following level set and BESO approaches. They all use filtering methods with mesh independency to converge to the desired value smoothly.

Unless the problem is convex it is very hard to claim that optimal design is reached. User generally decides on the number of iterations due to time constraints and there are always better solutions with decreasing profit until the global optimum is reached.

Basic cantilever beam with single load problem can be taken into consideration for a comparison case for level set and SIMP methods. Level set topology optimization is performed by a basic 2D matlab code on the other hand SIMP method is implemented in Catia v6. Level set example converges in 101 iterations whereas SIMP reaches to a very similar shape in 50 iterations.
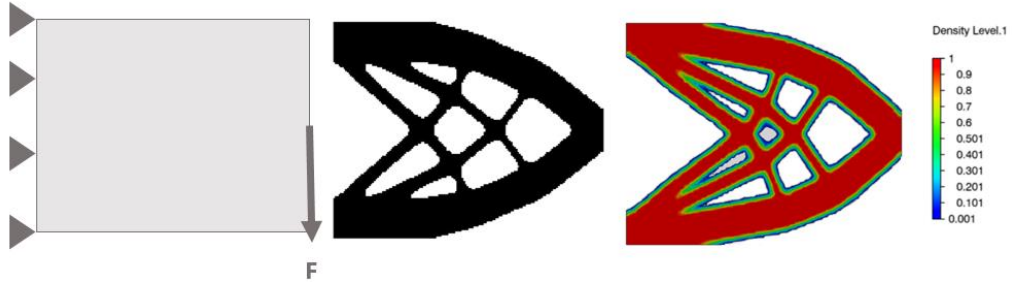
Figure 1.2. Comparison of level set solution created by matlab code (Appendix A) and SIMP method

1.4. Optimizers

Sequential Quadratic Programming (SQP) simplifies the nonlinear problem in ssteps by solving quadratic sub problems. It can be used both in line search and trust-region frameworks. It is a great tool to solve dense nonlinear problems but method incorporates several derivatives, which likely need to be worked analytically in advance of iterating to a solution.

Hybrid Cellular Automata (HCA) is first introduced by Khandelwal, Kapil & Tovar, Andres [46] for cellular automaton for nonlinear topology. It is inspired by bone structures. In bone development outer boundary mineralized cells are developed and HCA uses the same principle. Only surface elements change their densities during optimization process.

Methods of moving asymptotes (MMA) is introduced by Svanberg in 1987 in his study "the method of moving asymptotes-a new method for structural optimization". [47] It is extended for globally convergence in 2002 by Svanberg [48]. They are extremely reliable optimization engines and they have been in use for many years.

1.5. Literature background of Additive Manufacturing

Additive Manufacturing (AM), also known as three-dimensional printing (3D printing), has been studied for decades. A three-dimensional printing is invented in 1984 by Charles W.Hull from 3D Systems Corp. The machine is named Sterolithgraphy Apparatus [32]. Technology was very expensive at the time, so it was not suitable for the general market in the early days, however; with the advent of the 21st century, costs have decreased dramatically that enabled 3D printers to enter into many industries.

A three-dimensional printer works like a standard inkjet printer. However, a three-dimensional printer uses material to create a 3D object rather than printing layers of ink on paper [33]. The term Additive Manufacturing involves many technologies containing sub-sets such as 3D printing, layered manufacturing, direct digital manufacturing (DDM), rapid prototyping (RP), and additive fabrication.

Additive Manufacturing has already been used to make some niche products in many industries. Recently, the terms 3D printing and Additive Manufacturing can be used interchangeably. The term AM is the technology of overlapping successive layers of thin material and producing a final three-dimensional product. Each layer is between about 0.0254 and 2.54 mm thick[34].

A common variety of materials can be used such as metals, plastics, rubbers, resins, glass, ceramics and concrete [32]. It refers to the application of rapid prototyping technology. This is the first application for Additive Manufacturing that helps increase market entry and innovation. It can be called the process of quick prototyping a part or finishing the product. This section is further investigated/tested before mass production process. Most of the commercial 3D printers are operationally similar.

Table 1.1. *Additive manufacturing applications and benefits*

Industry	Applications	Benefits
Aerospace	Fast Prototyping/Test projects Aeronautical Components Weight reduction High temperature Components Space Components	No Shape limitaitons Reduce required workshop processes Reduce assembly requirements Space manufacturing for space stations Local editing inside of the part Reduces cost and weight
Automative	Fast Prototyping/Test projects Automative Components Weight reduction Heat Transfer components for cooling	Reduce assembly requirements Local editing inside of the part Reduce Repair cost Effect the shape overall of vehicles Reduces cost and weight Improve quality and manufacturing time
Machine Tool manufacturing	Fast Prototyping/Test projects Reduce raw material volume Improve packaging	Lighter and fast manufacturing Quick responses to change and implementation
Medical & Dental	Fast Prototyping/Test projects Custom implants Multimaterial organs , bones, body parts Teeth replacement with precision Orthodontic titanium components	Reduce operational time and cost Fast manufacturing and implementation Harmony with living cells through porus structure Harmony of multimaterials for different purposes
Civil Engineering/Construction	Fast Prototyping/Test projects Geometry precision on buildings Metalic Bridges and supports Truss structures Metallic connection components Mock up manufacturing	Mock up for review for customer needs Short construction time Reduce weight and construction material Build temporary constructions fastly
Food	Chocolate cake and candy Coffee mug decoration	Customization on shapes and images

The printer uses a computer-aided design (CAD) to convert the design into a three-dimensional object. The design is then divided with respect to z-axis with several two-dimensional sections that tell the three-dimensional printer where the material layers are to be placed. There are two kinds of Additive Manufacturing such as Powder Bed Fusion (PBF) processes and Directed Energy Deposition (DED) processes.

1.5.1. Powder Bed Fusion

There are various Powder Bed Fusion processes. The most common ones are listed below;

- Direct Metal Laser Sintering (DMLS)
- Electron Beam Melting (EBM)
- Selective Heat Sintering (SHS)
- Selective Laser Melting (SLM)
- Selective Laser Sintering (SLS)

A laser or electron beam is used by Powder Bed Fusion processes that melts and combines the material powder together. A vacuum is required by Electron Beam Melting methods. It can also be used with metals and alloys in the design of functional parts. All PBF processes involve the spreading of the powder material to the previous layers [35].

There are different processes to achieve this, involving a blade and a roller. A hopper under the bed provides fresh material. Selective Laser Sintering machines are composed of three components such as a heat source to fuse the material, a process to control this heat resource and a mechanism adding new layers of material over the previous [35]. Direct Metal Laser Sintering is very similar to Selective Laser Sintering. However, it uses metals and not plastics. The mechanism sinters in powder layer by layer. Selective Heat Sintering differs from other processes in using a heated thermal print head to fuse powder material together [35]. Furthermore, SHS uses thermoplastics powders. They function as support material. The application of a thermal print head and not a laser has the advantage of reducing the heat and power levels as needed. Selective Laser Melting is usually faster than Selective Laser Sintering, however; it needs to use an inert gas and has higher requirement of energy. Thus, it has poor energy efficiency between 10-20 % [35].

Any powder based material can be used by The Powder Bed Fusion process, in which some metals and polymers used are:

SHS: Nylon,

DMLS, SLS and SLM: Stainless Steel, Titanium, Aluminum, Cobalt Chrome, and Steel,

EBM: Titanium, Cobalt Chrome, Stainless Steel, Aluminum and Copper.

In short, to mention the advantages of Powder Bed Fusion; it is not relatively expensive. It can be used for visual models and prototypes. Also, it can be applied on integrated support structure. Disadvantages: it is relatively slow speed especially SHS; it is size limitations and high power usage; finally, it lacks structural properties in material.
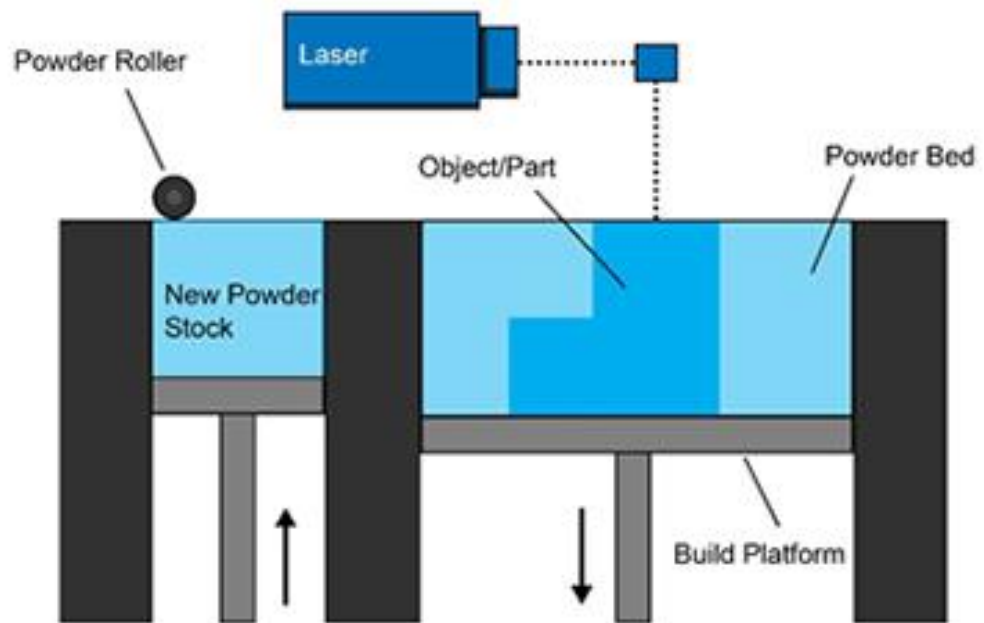
Figure 1.3. Powder bed fusion mechanism

1.5.2. Directed Energy Deposition

Directed Energy Deposition (DED) contains a wide terminology. Some of those are laser engineered net shaping, directed light fabrication, direct metal deposition, and 3D laser cladding [35]. A more complex printing process commonly used to repair or add additional material to existing components. DED machine covers a nozzle installed on a multi axis arm that mounts fused material onto the specified surface, where it solidifies. It works in a similar way to material extrusion, however; the nozzle is not set to a specific axis and also can drive in multiple directions. The material that can be deposited from any angle because of 4 and 5 axis machines are fused upon deposition with an electron or laser beam. The operation is used with polymers, and ceramics. However, it can be frequently used with metals, in the form of either powder or wire. Typical formations involve repairing and maintaining structural components.

Additionally, the Directed Energy Deposition method applies material in wire or powder form. Wire is less sensitive because its pre-formed nature, however; it is more material efficient when used with powder because only required amount of material is applied [35]. The Electron Beam Melting process uses metals, but it does not use polymers or ceramics;

Metals: Cobalt Chrome, Titanium.

Shortly, DED has the capability to provide grain structure to a high degree that contributes to the process of repair work of high quality functional parts. A trade-off occurs between surface quality and speed, even with repair applications, velocity can frequently be sacrificed for high accuracy and pre-decided microstructure[35]. Disadvantages: it has limited types of materials to work with.
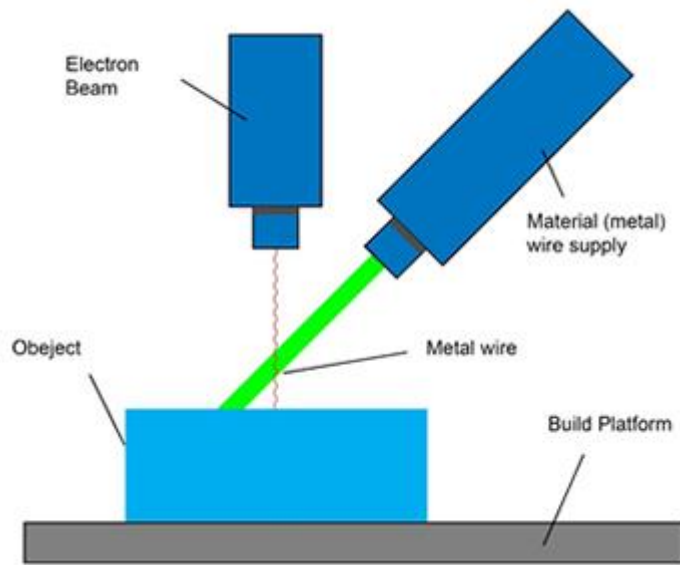
Figure 1.4. Wire supply with Electron beam heat source

1.6. Previous structural studies based on lattice structures with AM

A new method is proposed to optimize structural parts; graded lattice structure, the same can be achieved as in topology optimization with lattice structures under the same load constraint, and without overall volume loss.

Asymptotic homogenization with the combination of lattice structures provide new capabilities in optimization era. Maintaining the overall volume while decreasing weight provide many advantages when compared with traditional SIMP optimization. It provides not only high stiffness due to inertia but also capabilities to decrease weight without overall volume change.
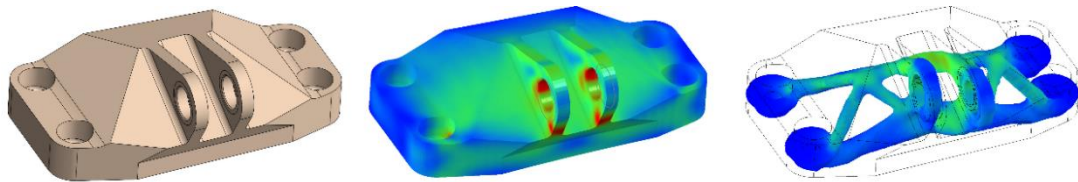
Figure 1.5. Traditional Topology Optimization with SIMP method
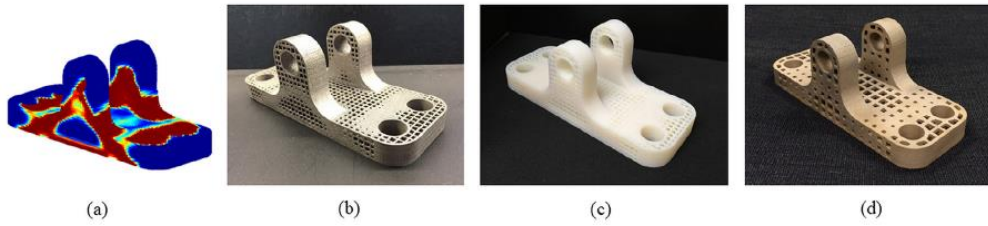
Figure 1.6. Overall lattice Optimization. (a) Load Paths; (b) Printed EOS DMLS Bracket; (c) Printed Polyjet Bracket; (d) Printed ExOne M-Flex Bracket [22]

Anders Clausen, Niels Aage, Ole Sigmund, show in their study [8] that coating approach offers no stiffness improvement but a strongly improved buckling load, which is an important element of structural stability, can be provided with an adaption of topology optimization to AM.
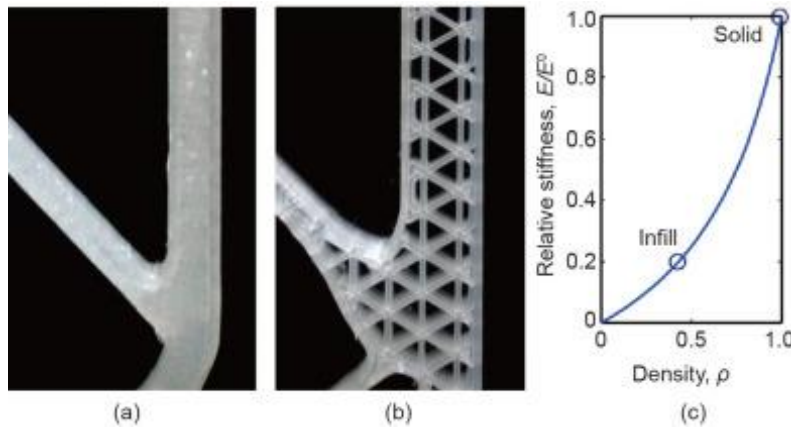
Figure 1.7. Solid versus Porous Components [8]

Also Westermann's physical tests [7] on a beam model shows that optimized infill generated provides great stiffness improvement with the same amount of material used. As shown in Figure 1.8, the beam is supported on the bottom at two ends while a downward force is applied on the top at the middle.
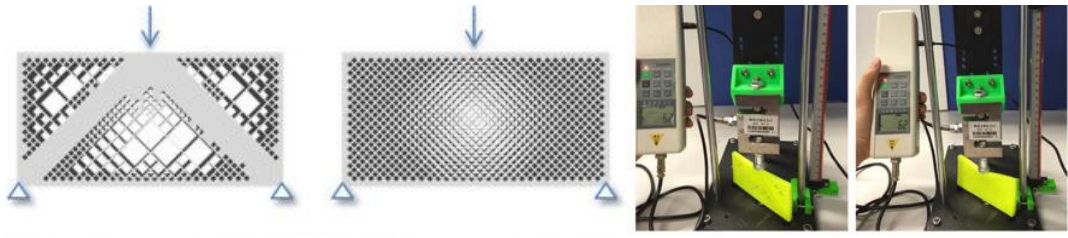
Figure 1.8. Optimized infill geometry and test bench [7]

Dawei Li, Wenhe Liao, Ning Dai and Yi Min Xie [6] compared the stiffness of a wing rib stiffness in their study. They presented results for different optimization strategies that are truss structures, the classical topology optimization method (SIMP) and CGLS with lattices method.
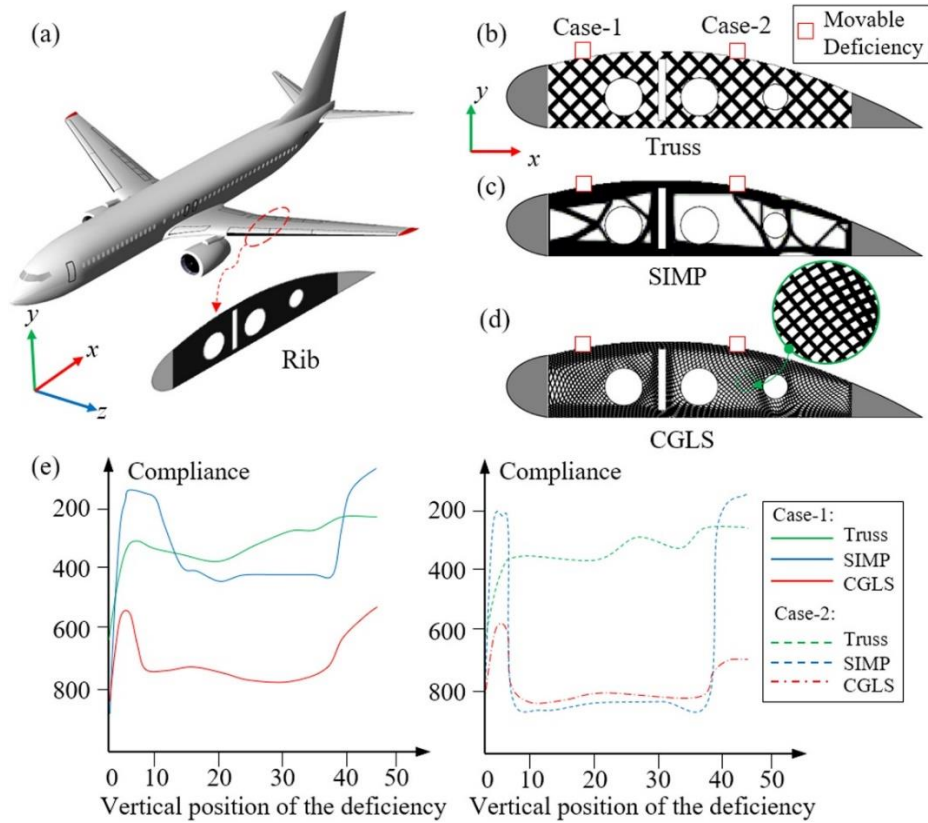
Figure 1.9. Stiffness Comparison of truss structure, the classical topology optimization method (SIMP) and CGLS with lattices method. [6]

15

Stephen Daynes, Stefanie Feih, Wen Feng Lu and Jun Wei [5] compared design stiffness of different designs with respect to "p" (penalty factor that accurately describes the lattice) and overhang angle constraint. The problem is set as a compression point in the middle and four support at corners of square. The agreement between calculated FEA and experiment shows that designed part has more stiffness than expected.
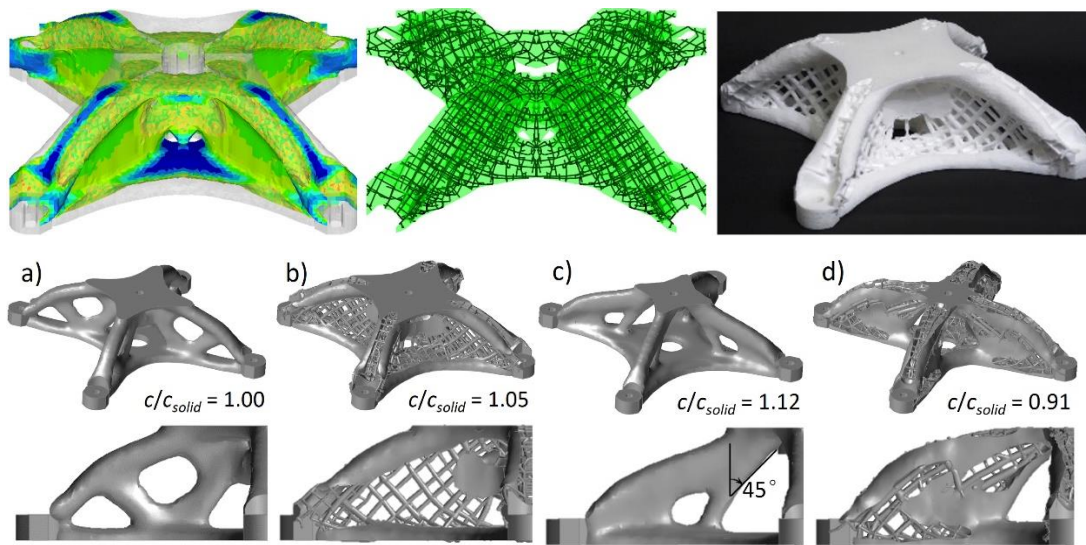
Figure 1.10. Influence of the 45 degree overhang constraint on compliance showing; (a) p=4, (b) p=1.8 , (c)p=4 with 45° overhang angle constraint and (d) p=1.8 with 450 overhang constraint.

CHAPTER 2

METAL ADDITIVE MANUFACTURING

Additive manufacturing (AM) increases its market value in the last decade with the release of its patent value. It continuously increases its value in different industries both amateur and professionals. The popularity grows day by day with technology growth in different materials and processes. It eliminates many of manufacturing constrains and gives freedom to designers in many perspectives during design process in both internal and external structural members. This freedom provides greater opportunities on shape during optimizing a geometry of components and improve mechanical properties.

In addition to these opportunities mentioned above, it also eliminates all manufacturing processes, labor and transportation between manufacturing shops. It gives opportunity to manufacture structural parts with only pushing a single button. This potential will further increase the usage of AM for a greater range of engineering applications.

One of the unique capabilities that AM brings to our life is infill structures. Infill, in other words solidity ratio, is simply a repetitive structure used to take up space inside the geometry. It is extruded in a designated percentage and pattern, and provides the part integrity with savings in raw material.

Additive manufacturing (AM) produces components by partially/fully melted layers of powder, metal wires, and ribbons. Raw materials are melted by fusion (electron beam, laser, and electric arc), solid state (ultrasonic, cold consolidation) or any other focused heat source. We can mainly divide additive manufacturing material feed methods into three that are powder bed, powder blown and wire.

Table 2.1. *Comparison of capabilities with respect to various AM techniques*

Source	Method	Resolution	Deposition Rate	Power Efficiency	Coupling Efficiency	Cleanliness	Cost	Surface Finish	Total
Laser	Powder Bed	2	-1	-1	-1	0	-1	3	**1**
	Powder Blown	1	2	-1	-1	0	0	1	**2**
	Wire	0	2	-1	-1	-1	-1	0	**-2**
E-Beam	Powder Bed	0	1	2	2	2	-1	1	**7**
	Wire	-1	2	2	2	1	1	0	**7**
Arc	Wire	-1	3	2	2	-1	3	-1	**7**

2.1. Current Additive Manufacturing Technologies

Powder Bed Fusion and Directed Energy Deposition processes are the two main metal additive manufacturing technologies in today's world and both divided into two main sub-technologies.
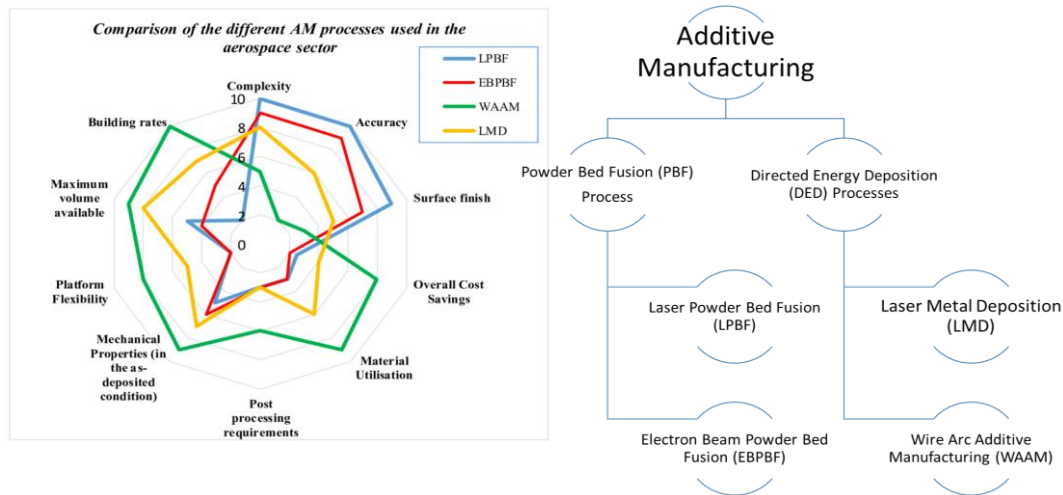
Figure 2.1. Current AM Technologies and Their Capabilities

Powder Bed Fusion process technology manufacture parts by melting powders with the help of a power source (EBM or Laser). Required areas of spread powder on build plane are melted by a power source and a new layer of powder is spread. This process

is repeated until the part is manufactured. Ceramics, plastics, glass or metal alloys can be used as powder raw materials. Stainless steel and titanium are two of the most popular powder raw materials due to their tough milling characteristic.

Two stages of heating are processed during electron beam powder bed deposition manufacturing. The two-stage heating prevents charging of the powder particles. Powder particles are preheated to sinter in the first stage and the heat density is increased to melt the particles in the second stage. When compared to laser, electron beam selective melting with powder bed deposition technique has greater advantages which are:

-Electron beam can provide smaller diameter of focused heat that increases precision during manufacturing process when compared to electromagnetic wave of light.

-Electron beam electric consumption is very low and efficiency of beam generation is very high when compared to laser.

-Heat transfer ratios/beam coupling on the work piece or powder material efficiency is better than laser.

-Focus location and power of beam can be controlled without any moving mechanism.

-Electron beam does not need oxygen for the process thus it has capability to work in vacuum that provides clean environment.

- Even though electron beam printers are expensive in the initial investment, it is cheaper to operate in regards to raw material and electric consumption.

Powder bed deposition brings good utilization of powders, precision and surface finish, high overhang angle, capability to build very complex shapes. However, it has some disadvantages such as low build rates, requirement of flat base and low build volume.

2.2. EBM with Arcam Q20 EBM

Arcam Q20 is one of the electron beam powder bed fusion machine available today. Electron beam melts the metal powder layer by layer to build the metal component. Multiple points can be melt at the same time with MultiBeamTM technology.

Figure 2.2. *ARCAM Q20 Overall* [12]

The powder bed and printing zone is low pressurized, nearly vacuum, with helium gas to provide clean and controlled environment. It has defect detection sensor and auto-calibration.

Table 2.2. *Build Specifications of Arcam Q20*

Max. Build Size (Diameter/Height)	350x380mm
Min. Beam Diameter	180 μm
Repositioning Time	10ms
Translation speed,	melting Continuously variable
Vacuum Base Pressure	$1x10_{-4}$ mbar
Raw materials	Ti6Al4V, Titanium Grade 2, Cobalt-Chrome ASTM F75, Nickel Alloy 718
Max. Beam Power	3000W
Max. EB translation speed	8000 m/s

2.3. Additive Manufacturing of Titanium Alloys

Titanium alloys are one of the most advanced materials and has a very critical role to improve performance of aerospace vehicles due to their outstanding mechanical, heat resistant and anti-corrosion behavior. Their low density, high strength features are suitable for various applications. However, their high strength mechanical properties also prolong the production processes of both raw materials and detail mechanical components.

Numerous studies have been conducted including powder methodology, near net shape production to decrease consumption of raw material. Reduction on buy to fly ratio decreases the costs and makes titanium well suited to additive manufacturing.

2.4. Mechanical Properties of Ti-6Al-4V

There are various standards related to production and mechanical properties of raw Ti-6Al-4V accepted by aerospace authorities. For example, SAE AMS4999A covers the titanium alloy direct products Ti-6Al-4V annealed. The properties of Ti-6Al-4V in Table 2.3 is described in Metallic Materials Properties Development and Standardization (MMPDS-11) Handbook written in 2016.

On the other hand, it is very hard to meet required qualifications on additive manufacturing. Production malfunctions, manufacturing type and small variations in environment cause unexpected effects on mechanical properties of the final component. Mechanical properties of various AM processes can be shown in Figure 2.3

Table 2.3. *Material Specifications and standards*

Alloy	Specification	Form
Ti-6Al-4V	AMS 4904	Sheet, strip, and plate
Ti-6Al-4V	AMS 4911	Sheet, strip, and plate
Ti-6Al-4V	AMS 4920	Die forging
Ti-6Al-4V	AMS 4934	Extrusion
Ti-6Al-4V	AMS 4935	Extrusion
Ti-6Al-4V	AMS4962	Casting
Ti-6Al-4V	AMS 4965	Bar
Ti-6Al-4V	AMS 4967	Bar
Ti-6Al-4V	AMS 4928	Bar and die forging
Ti-6Al-4V	AMS 4962*	Investment casting
Ti-6Al-4V	AMS 4992	Investment casting
Ti-6Al-4V	AMS 6930	Bar
Ti-6Al-4V	AMS 6931	Bar and Die Forging
Ti-6Al-4V	AMS 6945	Sheet and Plate
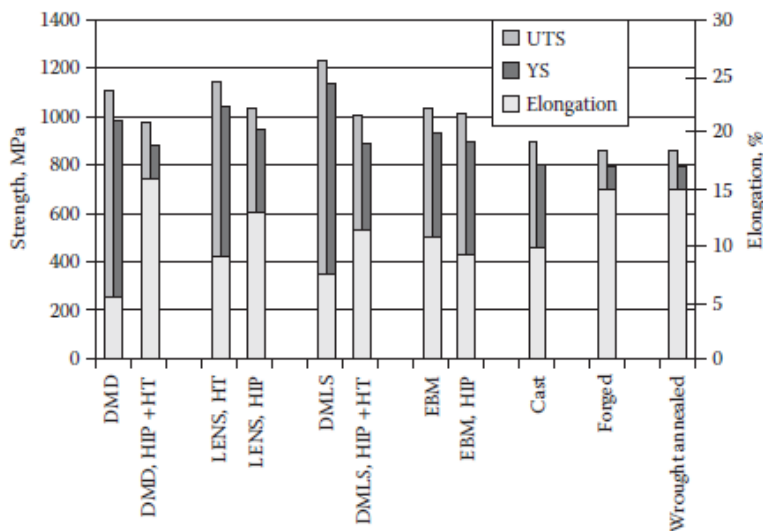
Figure 2.3. Tensile strength, yield strength, and elongation of Ti-6AI-4V alloy built different AM processes [4]

Tensile specimens are built with respect to varied X- axis, Y-axis and Z-axis layers in our facility by Yiğitbaşı S.T. (2018) [3].
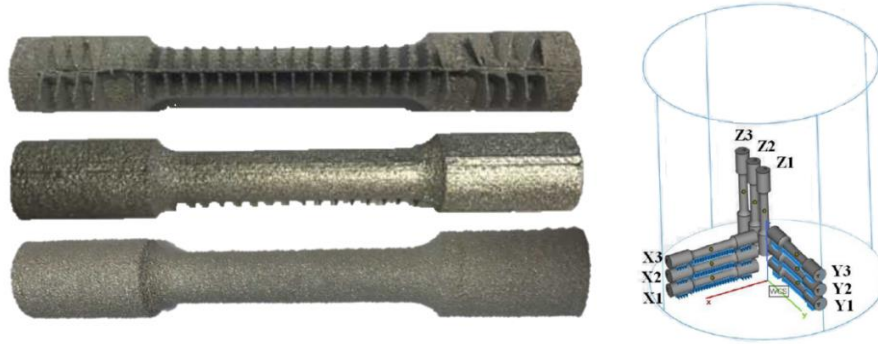
Figure 2.4. Manufactured tensile specimens with respect to build directions, X, Y and Z direction from above to below in Yiğitbaşı S.T. study. [3]

The mechanical properties have variations related to build directions. The difference between yield strength from lowest, X-axis to highest, Z-axis, is nearly 88Mpa in nominal. The comparison is provided in Table 2.4.

Table 2.4. *Mechanical properties from Yiğitbaşı S.T's study that compared with other sources* [3]

	X Samples	Y Samples	Z Samples	ARCAM Ti6Al4V Powder*	Cast Ti6Al4V Material**	Wrought Ti6Al4V Material***
Ultimate Tensile Strength [MPa]	967±29	988±13	1023±21	1020	860	930
Yield Strength (Offset 0.2%) [MPa]	852±16	895±14	940±23	950	758	860
Young's Modulus [GPa]	155±17	136±17	158±22	120	114	114
Elongation [%]	19±5	15±4	10±2	14	>8	>10

* Given by ARCAM Company, ** Required values according to ASTM F1108, *** Required values according to ASTM F1472

The most comprehensive study related to material properties of electron beam melting Ti-6Al-4V is done by National Aeronautics and Space Administration. In depth material characterization of electron beam melted Ti-6Al-4V is done by Susan Draper, Brad Lerch, Richard Rogers, Richard Martin. Ivan Locci, Anita Garg [2] using very similar ARCAM A2X EBM machine including tensile, fracture toughness, fatigue crack growth, low cycle fatigue, high cycle fatigue at different temperatures. Also the mechanical properties are compared with conventional annealed Ti-6Al-4V. The dynamic properties are found as E=118 GPa (Elastic Modulus), G=45.7 GPa (Shear Modulus/ Modulus of rigidity) and υ=0.29 (Poisson's ratio). Mechanical properties at different temperatures are shown in Table 2.5.

Table 2.5. *Experimental mechanical properties from NASA technical report.* [2]

Sample	Build	Ez, GPa	Proportional limit, MPa	0.02% yield, MPa	0.2% yield, MPa	Ultimate strength, MPa	Failure strength, MPa	Failure strain, percent	RA, percent
−196 °C									
25	1-1-2	129	1530	1534	1702	1744	1671	10.9	20
43	1-1-2	126	1582	1582	1696	1731	1695	8.1	13
105	1-2-2	126	1579	1583	1695	1733	1682	9.8	17
122	2-4-1	124	1407	1416	1555	1608	1607	5.8	6.5
170	2-4-5	121	1452	1455	1549	1605	1565	12.2	18
191	2-4-9	120	1478	1478	1589	1646	1633	8.8	12
−101 °C									
28	1-1-1	128	1272	1283	1336	1394	1289	14.0	26
55	1-1-4	124	1243	1258	1324	1387	1301	14.3	22
95	1-2-2	127	1266	1276	1339	1406	1356	12.4	19
147	2-4-3	121	1180	1187	1243	1300	1274	13.1	18
160	2-4-4	119	1191	1196	1237	1287	1238	13.7	22
198	2-4-8	122	1117	1160	1244	1304	1208	15.7	27
20 °C									
16	1-1-2	125	------	------	------	------	------	------	------
65	1-1-4	124	974	998	1028	1126	1000	21.5	30
67	1-1-4	122	980	1000	1025	1122	998	21.0	31
115	1-2-1	126	967	992	1024	1140	1014	20.7	30
135	2-4-2	118	908	929	960	1042	962	20.2	28
173	2-4-6	118	914	935	965	1051	960	20.7	29
186	2-4-6	118	928	941	972	1048	1027	9.8	11
H1	------	118	865	896	958	1058	970	13.6	12
H3	------	119	831	866	950	1057	992	13.2	14
H11	------	118	866	901	977	1081	1064	14.4	13
149 °C									
34	1-1-2	118	745	788	813	948	676	18.1	49
78	1-1-3	117	768	798	819	941	627	22.0	55
86	1-2-2	117	792	804	817	944	834	18.2	43
141	2-4-1	111	701	722	747	841	576	22.0	58
153	2-4-5	113	689	730	760	854	753	17.1	50
183	2-4-9	113	729	749	775	861	540	21.1	39

Various studies do not converge on a single value for yield and ultimate strength of the titanium alloy Ti-6Al-4V. As a result, the lowest value 831 Mpa for yield strength with 967 Mpa for ultimate strength are taken into consideration in the following optimization process.

CHAPTER 3

THEORY

3.1. Conventional Optimization Types

Optimization procedures can be divided into three standard practices in regards to their usage that are sizing, shape and topology optimization procedures. Figure 3.1 shows how much final shapes changes with respect to optimization procedures. The first geometry represents the initial configuration before optimization process and the second geometry shows the final geometry of the object after the optimization.
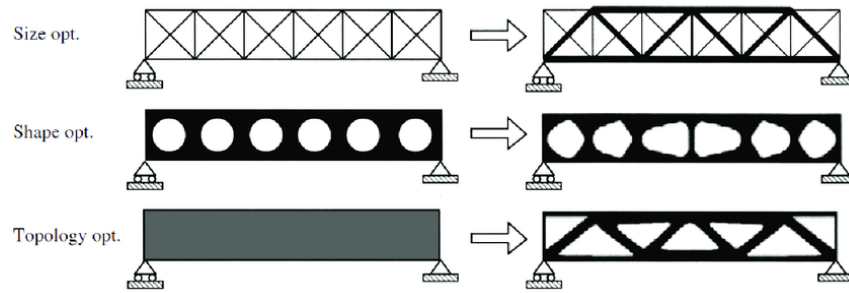
Figure 3.1. Depiction of sizing, shape and topology optimization procedures [36]

Topology optimization is a very strong tool to generate a new concept constructing design proposal for a new component. Starting with maximum allowed design volume for the component and with the boundary conditions, the optimization procedure creates a new material distribution by determining load patterns and removing unnecessary parts. This design proposal satisfy all mechanical requirements while creating a weight-optimal design.

The main criteria for selecting optimization type is the production capabilities. Each optimization type have their advantages and disadvantages. Shape or in other words parameter optimization, is most used one in the industry due to ease of producibility and nowadays however the use of topology optimization is growing together with the

development of 3D printing capabilities. The production methods also affect the topology optimization types. Liu and Ma [31] shows the differences of machining oriented and injection molding/casting oriented topology optimization methods clearly in their research.

Figure 3.2. Dragon Tree example with traditional topology optimization [13]

Topology optimization algorithms can be divided into two main groups which are the controller based algorithm for standard problems and the sensitivity based algorithm for extended problems. Some of the main differences between sensitivity based optimization algorithm and controller based algorithm are the following:

1. Elements with intermediate densities (grey elements): The sensitivity based algorithm has some elements in the final design containing intermediate densities (grey elements), whereas the controller based algorithm leads to the elements being either void (density very close to zero) or solid (density equal to one) in the final design.

2. Number of optimization iterations: The controller based algorithm uses 15 optimization iterations by default. For the sensitivity based optimization algorithm, the number of iterations is unknown before the optimization starts, but normally the number of optimization iterations is around 30 to 45.

3. Analysis types: The sensitivity based algorithm supports the responses of linear static (non-conservative forces) and linear eigen-frequency (not allowed to be pre-stressed) finite element analysis. On the other hand, the controller based algorithm also supports non-linear static analysis such as contact simulation, even when the contact zones are on the surfaces of the design space. The sensitivity based algorithm supports geometrical nonlinearities (NLGEOM) and some non-linear materials are also supported. Other non-linearities in the sensitivity based algorithm are not supported. Furthermore, prescribed displacements are allowed in the CAE model for static topology optimization. However, prescribed displacements are not allowed for modal and frequency response analysis. Generally, laminate materials cannot be designed in topology optimization.

4. Objective and constraint types: The sensitivity based algorithm can have one objective function and several constraints where the constraints are all inequality constraints. The objective and the constraints can be based upon the stiffness, displacements, reaction forces, internal forces, eigen-frequencies and material volume (material weight). On the other hand, the controller based algorithm has the compliance as objective and the material volume as an equality constraint.

5. Algorithms: For sensitivity based topology optimization task a general optimization algorithm is integrated. This algorithm uses the sensitivities of the design variables with regard to the objective function and the constraints. Tosca Structure uses an algorithm based on the Method of Moving Asymptotes from Krister Svanberg (Sweden). It is not necessary to calculate the sensitivities for the Tosca Structure controller-based strategy. The controller uses the strain energy and the grid point stresses as input data.

In topology optimization, a variety of combinations of objective functions and constraints can be selected. Standard formulation using the efficient controller based optimality criteria algorithm is: Maximize stiffness (objective function) with a volume constraint (constraint). All other types of objective functions and constraints can be

applied using the sensitivity-based algorithm. Feasible objective functions and constraints are valid for sensitivity-based algorithm which are:

- Center of gravity
- Displacement (absolute or relative)
- von Mises Stress
- Moment of inertia
- Rotations
- Reaction forces (absolute or relative)

- Reaction moments (absolute or relative)
- Internal forces (absolute or relative)
- Internal moments (absolute or relative)
- Eigen frequencies
- Material Volume
- Total stiffness

3.2. Minimum Compliance Design

Minimum compliance (maximum stiffness) is a natural starting point for conceptual studies. Problem formulation is expressed using the basic equations of elasticity and energy principles. Mathematically, problem is indeed a boundary value problem for an elastic body subjected to external forces. The external surface is sum of the boundary with displacements u (Γ_u), boundary with tractions t (Γ_t) and free surfaces that has zero tractions.
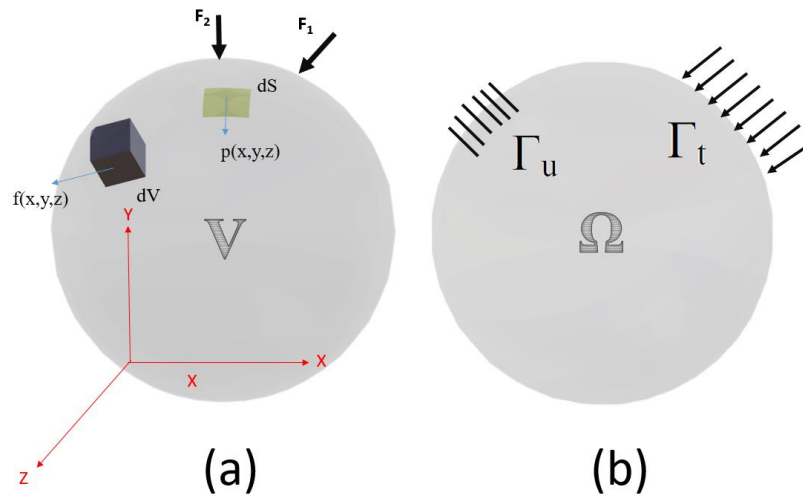

Figure 3.3. a- Elastic body subjected to external forces, b- 3D domain with surface forces

The elastic body confines a domain having volume V and surface S that is a part of largest domain Ω in R3. Optimal design aims to find the optimal choice of stiffness tensor E_{ijkl} in reference to Ω. Now assume virtual displacement δu occurs from equilibrium state of the body. Some assumptions are needed to write virtual work equation. Dissipative effects are neglected (reversible body). Interaction between temperature and deformation is neglected (deformation in isothermal course). Kinetic energy and inertia forces are neglected (process is quasi-static). Finally, forces on deformed and undeformed volume are assumed as equal.

The external forces can be expressed as volume forces (f_i), distributed surface tractions (p_i), and concentrated forces (F_i). External work can be described as summation of the forces effecting elastic body.

External work done by volume forces can be described as integral of normal force f, against the change state of displacement δu through the volume. External work done by surface tractions can be described as integral of surface tractions p, against the change state of displacement δu through the all surface and work done by concentrated forces can be described as integral of concentrated forces F, against the change statement of displacement vectors for points of action of concentrated forces δu^0.

External work of an elastic body, due to virtual displacements and external forces becomes [49]:

$$\delta W = \int_V f_i \delta u_i \, dV + \int_S p_i \delta u_i \, dS + F_i \delta u_i^0 \qquad (3\text{-}1)$$

External work also can be expressed in vector notation ;

$$\delta W = \int_V f^T \delta u \, dV + \int_S p^T \delta u \, dS + F^T \delta u^0 \qquad (3\text{-}2)$$

where,

f^T : Vector of volume forces

p^T : Vector of surface tractions

F^T : Vector of concentrated forces (F_1^T, F_2^T ……F_n^T)

u_i^0 : Vector of displacement vectors for concentrated forces

u^T =[u v w] : Displacement vector (u, v, w)

Assume that the elastic body is subjected to a virtual displacement then the virtual work done due to surface and body forces, eliminating concentrated forces F, can be expressed as [50]

$$\delta W = \int_V F \delta u \, dV + \int_S p^T \delta u \, dS \qquad (3\text{-}3)$$

.

If a small cut is made at a given position in the domain with the unit normal n to the resultant surface, there is a force exerted by the material into which the unit normal n points on the material from which the unit normal n points. This force measured per unit area of surface is the traction vector p. For the mixed boundary value problems, Cauchy stress tensor, σ_{ij}, relates the unit normal to the small cut to the traction vector according to

$$p^T = (\sigma_{ij} \, n_j) \qquad (3\text{-}4)$$

surface tractions p in (3-3) can be replaced with (3-4) and it becomes

$$\delta W = \int_V F_i \delta u_i \, dV + \int_S \sigma_{ij} n_j \, \delta u_i \, dS \qquad (3\text{-}5)$$

By means of the divergence theorem, surface integral can be transformed to a volume integral, thus it becomes:

$$\delta W = \int_V F \delta u \, dV + \int_V (\sigma_{ij} \delta u_i)_{,j} \, dV \qquad (3\text{-}6)$$

(3-6) can be manipulated as the following;

$$\delta W = \int_V F_i \delta u_i \, dV + \int_V \left(\sigma_{ij,j} \, \delta u_i + \sigma_{ij} \, \delta u_{i,j} \right) dV$$

(3-7)

In equilibrium condition, summation of concentrated forces and Cauchy stress tensors should be zero that is defined as the following in index notation;

$$\sigma_{ij,j} + F_i = 0$$

(3-8)

Strain, ε_{ij}, and displacement u_i relations are given by;

$$\varepsilon_{ij} = \frac{1}{2} \left(u_{i,j} + u_{j,i} \right)$$

(3-9)

(3-8) can be rewritten with $\sigma_{ij,j} = -F_i$ from (3-8) and since $u_{j,i} = u_{i,j}$ it can be concluded that $\varepsilon_{ij} = u_{i,j}$ from (3-9) and (3-7) becomes

$$\delta W = \int_V F_i \delta u_i \, dV + \int_V \left(-F_i \delta u_i + \sigma_{ij} \, \varepsilon_{i,j} \right) dV,$$

(3-10)

First part of second integral and first integral cancel each other and it becomes,

$$\delta W = \int_V \left(\sigma_{ij} \varepsilon_{ij} \right) dV$$

(3-11)

Stress tensor can be defined as multiplier of elasticity tensor of order four, E_{ijkl}, and strain tensor ε_{kl}

$$\sigma_{ij} = E_{ijkl} \varepsilon_{kl}$$

(3-12)

Therefore, (3-10) can be rewritten with the implementation of (3-11) as

$$\delta W = \int_V \left(E_{ijkl} \varepsilon_{kl} \varepsilon_{ij} \right) dV \qquad (3\text{-}13)$$

If the equilibrium state of internal virtual work is represented by 'a' and arbitrary virtual displacement by 'b' for an elastic body, then by means of energy bilinear form, the virtual work done by the elastic body (for a reference domain Ω) can be expressed as [51]:

$$\delta W(a,b) = \int_\Omega E_{ijkl}(x)\varepsilon_{kl}(a)\varepsilon_{ij}(b) \, d\Omega \qquad (3\text{-}14)$$

where x with $E_{ijkl}(x)$ indicates the optimal stiffness tensor.

Linearized form of strains $\varepsilon_{ij}(u) = \frac{1}{2}\left(\frac{\partial u_i}{\partial x_j} + \frac{\partial u_j}{\partial x_i}\right)$ and load linear form can be defined by [51]

$$l(a) = \int_\Omega f u d\Omega + \int_{\Gamma_T} t u dS \qquad (3\text{-}15)$$

Maximum global stiffness problem with linearized strains and the load linear form, $\min l(a)$, can be expressed as:

$$\begin{aligned} \delta W_E(a,b) = l(b) \quad for \; all \; b \in U \\ E \in E_{ad} \end{aligned} \qquad (3\text{-}16)$$

where U denotes the space of kinematically admissible displacement fields. Set of admissible stiffness tensors for design problem denoted by E_{ad} that consist of all stiffness tensors attaining the material properties of a given isotropic material in the set Ω_{mat} and no properties elsewhere. Moreover, it should satisfy $\int_{\Omega_{mat}} 1 d\Omega \leq V$ comes from limit of source.

The problems formed as (3-15) is generally solved by discretizing the problem with finite elements. There are two important parameters, fields of interest, that are displacement u and stiffness E. The same finite element mesh can be used for both displacement and stiffness fields. Stiffness is discretized as constant in each element.

Discrete form of (3-15) can be written using the displacement vector u and the force vector f,

$$\begin{aligned} &\min f^T u \\ &K(E_e)\, u = f, \\ &E \in E_{ad} \end{aligned} \qquad (3\text{-}17)$$

stiffness matrix, K, depends on the global level stiffness of the individual elements E_e in element e, numbered as $e=1,\ldots.N$, and it can be written as

$$K = \sum_{e=1}^{N} K_e(E_e) \qquad (3\text{-}18)$$

where K_e represent the global level element stiffness matrix.

The space should be filled with isotropic material and void (no material) during the determination of optimal placement of structure like black and white rendering of an image. It is black and white raster representation of the geometry in discrete form with finite element discretization. Optimal subset Ω_{mat} of material points is to be determined in reference domain Ω. It implies that the set E_{ad} problem (distributed, discrete valued, a 0-1 design problem) of admissible stiffness tensor formed by those tensors which are

$$E_{ijkl} = 1_{\Omega mat}\, E_{ijkl}^0 \text{ where } 1_{\Omega mat} = \begin{array}{l} 1 \; if \; x \in \Omega mat \\ 0 \; if \; x \in \Omega \backslash \Omega mat \end{array} \qquad (3\text{-}19)$$

$\int_\Omega 1_{\Omega mat}\, d\Omega = Vol\,(\Omega mat) \leq V$ where V denotes the limit material at disposal

However, this 0-1 problem commonly replaced with continuous variables rather than integer variables with penalty. Intermediate values of artificial density function is penalized similar to other approximations. Penalized, proportional stiffness model (Solid isotropic material with penalization model) can be formulated as:

$$E_{ijkl}(x) = \rho(x)^p E_{ijkl}^0 \quad p > 1 ,$$
$$\int_\Omega \rho(x) \, d\Omega \leq V; \qquad 0 \leq \rho(x) \leq 1, \quad x \in \Omega, \tag{3-20}$$

where p is the penalty parameter.

$\rho(x)$, density, is taken as design function and material properties of a isotropic material is denoted by E_{ijkl}^0. Density, that is called pseudo-density or artificial density in some references, represents the effectivity of the element in the domain such as $E_{ijkl}(\rho = 0) = 0$ and $E_{ijkl}(\rho = 1) = E_{ijkl}^0$. The usage of interpolation scheme like SIMP transforms the topology problem into a sizing problem with fixed domain. Minimum compliance problem can be written for SIMP interpolation case in continuum settings [51] as the following

$$\min_{u \in U, p} l(u) \tag{3-21}$$
$$a_E(u, v) = l(v), \; for \; all \; v \in U, \tag{3-22}$$
$$E_{ijkl}(x) = \rho(x)^p E_{ijkl}^0 \tag{3-23}$$
$$\int_\Omega \rho(x) \, d\Omega \leq V; \qquad 0 \leq \rho_{min} \leq \rho \leq 1 \tag{3-24}$$

The problem is bounded from below like $\rho_{min} = 10^{-3}$ to prevent singularity. Sizing variable "ρ" is built with stationary conditions for the Lagrange function with the help of Lagrange multipliers $\Lambda, \lambda^-(x), \lambda^+(x)$.

34

$$\mathcal{L} = l(u) - \{a_E(u, \bar{u}) - l(\bar{u})\}$$
$$+ \Lambda \left(\int_\Omega \rho(x) d\Omega - V \right)$$
$$+ \int_\Omega \lambda^+(x) \left(\rho(x) - 1 \right) d\Omega \qquad (3\text{-}25)$$
$$+ \int_\Omega \lambda^-(x) \left(\rho_{min} - \rho(x) \right) d\Omega$$

"$\bar{u}$" is the lagrange multiplier belonging the set U of kinematically admissible displacement fields that is valid for equilibrium constraint. Displacement fields are unique under the assumption of $0 < \rho_{min} \leq \rho$. "$u = \bar{u}$" condition must be satisfied for the conditions of optimality with respect to variations of the displacement. The condition for p becomes:

$$\frac{\partial E_{ijkl}}{\partial \rho} \varepsilon_{ij}(u)\varepsilon_{kl}(u) = \Lambda + \lambda^+ - \lambda^- \qquad (3\text{-}26)$$

with switching conditions $\lambda^- \geq 0, \lambda^+ \geq 0, \lambda^-(\rho_{min} - \rho(x)) = 0, \lambda^+(\rho(x) - 1) = 0$.

Equation (3-26) can be rewritten with intermediate densities $\rho_{min} < \rho < 1$

$$p\rho(x)^{p-1} E_{ijkl}\varepsilon_{ij}(u)\varepsilon_{kl}(u) = \Lambda \qquad (3\text{-}27)$$

It also states that strain energy density like left hand side term is equal to Λ and it is a constant value. It is very similar to fully stressed design condition in plastic design. It is expected that low stiffness areas have high energy. Density schema can be arranged [51] for each iteration as follows:

$$\rho_{k+1}$$
$$= \begin{cases} max\{(1 - \xi)\rho_k, \rho_{min}\} & if \ \rho_k B_K^\eta \leq max\{(1 - \xi)\rho_k, \rho_{min}\} \\ min\{(1 + \xi)\rho_k, 1\} & if \quad min\{(1 + \xi)\rho_k, 1\} \leq \rho_k B_K^\eta \\ \rho_k B_K^\eta & otherwise \end{cases} \qquad (3\text{-}28)$$

where ρ_k denotes the value of density variable in each step K and

$$B_K = \Lambda_K^{-1} p \rho(x)^{p-1} E_{ijkl}^0 \, \varepsilon_{ij}(u_K) \varepsilon_{kl}(u_K) \tag{3-29}$$

Here u_K is the displacement field of iteration step K, the variable η is a tuning parameter and ξ is a move limit. The values of them can be found by experiment to provide stable and fast convergence. They are taken as $\eta = 0.5$ and $\xi = 0.2$ typically [51].

Method of moving asymptotes (MMA) is a mathematical well suited programming algorithm for smooth, nonlinear optimization like sequential linear programming (SLP) and sequential quadratic programming (SQP). They transform the problem into simpler approximate sub problems and these problems are solved by dual method or by a primal dual algorithm. The solution of sub problem is used as next design in the iteration process. In the method of moving asymptotes, the function F with n variables x=(x_1, x_2, …. x_n) around a point x_0 can be formed as the following;

$$F(x) \approx F(x^0) + \sum_{i=1}^{n} \left(\frac{r_i}{U_i - x_i} + \frac{s_i}{x_i - L_i} \right) \tag{3-30}$$

where r_i and s_i are defined as

If $\frac{\partial F}{\partial x_i}(x^0) > 0$ then $r_i = (U_i - x_i^0)^2 \frac{\partial F}{\partial x_i}(x^0)$ and $s_i = 0$

If $\frac{\partial F}{\partial x_i}(x^0) < 0$ then $r_i = 0$ and $s_i = (x_i^0 - L_i)^2 \frac{\partial F}{\partial x_i}(x^0)$

The parameters U_i, L_i give vertical asymptotes for the approximation of F that give the name of the method and they are updated in each iteration.

3.3. Computational Procedure

The main process relies on the numerical calculation of the global distribution of the material ρ that is the design variable. The optimality criteria for the optimal topology is performed on single isotropic material. Computational process can be divided into

36

three main steps that are pre-process, optimization and post-process. We can list the computational process of topology optimization for load boundaries in the following steps:

Pre-processing the design volume and load cases of the model

- Creating a suitable reference design domain that covers volume constrains related to design.
- Determination of solid or void volumes (if exists) on design domain
- Constructing a fine finite element mesh for design domain. Note that size of the mesh directly effects the resolution of optimization.

Optimization

- Distribute the material homogeneously as an initial design

- Compute the resulting displacements and strains via finite element method.

- Compute the compliance of design in this iteration. If the conditions are satisfied or there is a marginal change from previous iteration, stop; else continue to the next iteration.

- Compute the density variable. Also calculate the Lagrange multiplier with inner loop for volume constraint.

- Repeat the iteration loop until conditions are satisfied.

Post- Processing of resultant geometry

- Interpret the optimal distribution of material to define shape.
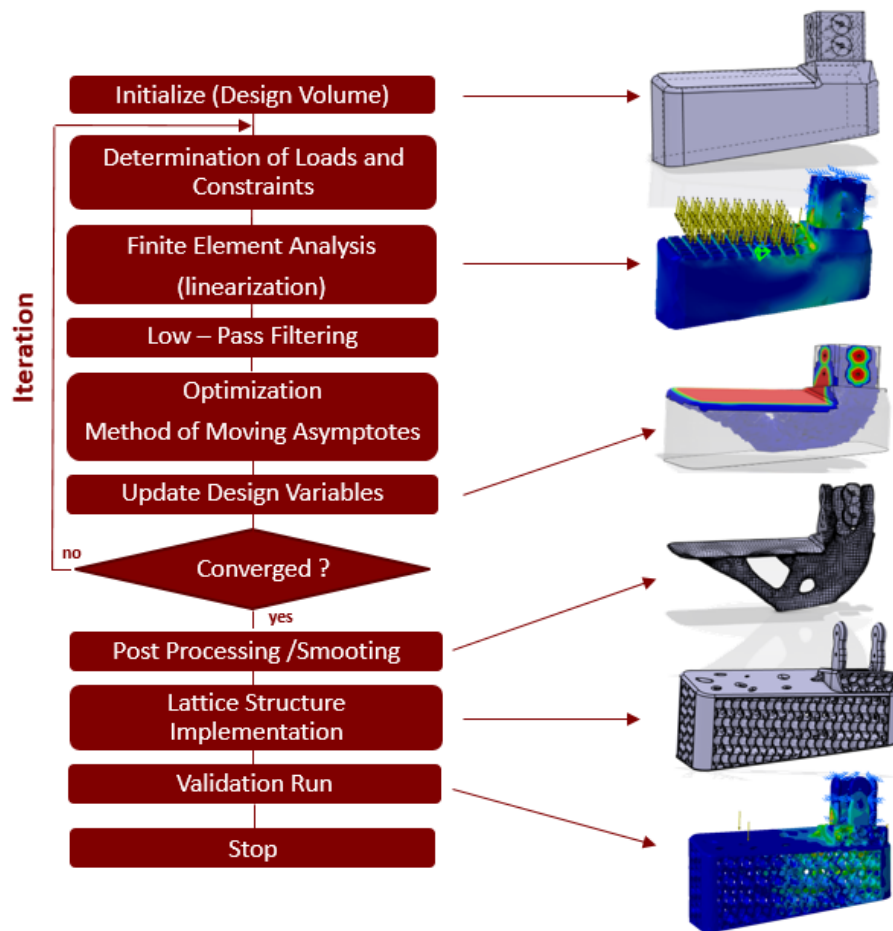
- Create a single, smoothed CAD model.

Figure 3.4. Design Process of topology optimization with lattices

Implementation of Lattice Structure

- Post-processed load boundary geometry is used as a template for lattice geometry
- Selected lattice structure is implemented as an infill in the load boundary template.

Validation run

- Finite element analysis is performed on final geometry

3.4. Minimal Surfaces

Minimal surfaces have zero mean curvature. Minimal surfaces are parametrized as x=(u,v,h(u,v)) where they satisfy Lagrange's equation [53],

$$(1 + h_v^2)h_{uu} - 2h_u h_v h_{uv} + (1 + h_u^2)h_{vv} = 0 \qquad (3\text{-}31)$$

A plane is a trivial minimal surface, the catenoid and helicoid were the first discovered nontrivial solutions. Then skew quadrilateral is discovered as a solution of famous minimum bonding surface. Sphere is also a minimal surface which provides best surface-area/volume ratio. On the other hand, it is not qualified as a minimal surface in a sense used by mathematicians.

(a)   (b)   (c)   (d)
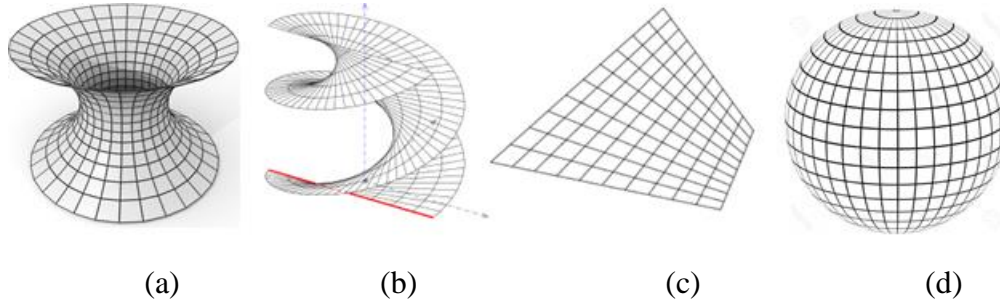
Figure 3.5. a- Catenoid, b- Helicoid, c- Skew Quadrilateral, d- Sphere

Isothermal parameterization is one of the tools that is used during surface parametrization. If the coordinate functions x_k are harmonic, minimal parametrization is satisfied. Thus, a minimal surface can be defined by a triple of analytic functions. Minimal surfaces can be defined as isothermal surfaces. Let Ø = $(\emptyset^1, \emptyset^2, \emptyset^3)$: $\mathbf{U} \in R^3$ be an arbitrary map. Ø is isothermal if and only if following equation is satisfied everywhere on $\mathbf{U}$;

$$(\emptyset_z^1)^2 + (\emptyset_z^2)^2 + (\emptyset_z^3)^2 = 0 \qquad (3\text{-}32)$$

If (3-30) is satisfied, $\emptyset$ is a regular parametrized surface if and only if following satisfied everywhere on **U**

$$|(\emptyset_z^1|^2 + |(\emptyset_z^2|^2 + |(\emptyset_z^3|^2 \neq 0 \qquad (3\text{-}33)$$

If **U** is simply connected, two paths between two points are continuously deformed into the other in U, we can conclude that

$$\emptyset^k = Re \int_{-\infty}^{\infty} \emptyset_z^k(z)dz \qquad for \ k = 1,2,3 \qquad (3\text{-}34)$$

However, for a meromorphic function of *h(z)*, i.e. a single-valued function that is analytic in all but possibly a discrete subset of its domain, and analytic function of *f(z)* function that can be locally expressed by power series. As long as *f(z)* has a zero of order $\geq m$ at every pole of *h(z)* of order m the above equations are analytic. It provides minimal-surface in terms of the Enneper-Weierstrass [52] parameterization, which is

$$
\begin{aligned}
\emptyset^1 &= Re \int_{-\infty}^{\infty} \frac{1}{2} h(z)(1 - g(z)^2)dz \\
\emptyset^2 &= Re \int_{-\infty}^{\infty} \frac{i}{2} h(z)(1 + g(z)^2)dz \qquad (3\text{-}35) \\
\emptyset^3 &= Re \int_{-\infty}^{\infty} h(z)g(z)dz
\end{aligned}
$$

It can be rewritten as triple equation as;

$$
\begin{aligned}
\emptyset_z^1 &= \frac{1}{2} h(z)(1 - g(z)^2)dz \\[2mm]
\emptyset_z^2 &= \frac{i}{2} h(z)(1 + g(z)^2) \qquad (3\text{-}36) \\[2mm]
\emptyset_z^3 &= h(z)g(z)
\end{aligned}
$$

As to the studies, Triply/infinitely periodic minimal surfaces were first described by H. A. Schwarz in 1865 [18]. His work was followed by his student, R. Neovius, with

new surfaces in 1883. Infinitely periodic minimal surfaces did not go further until the Alan Schoen, an American physicist, who contributed twelve new IPMS based on crystallographic cells[16]. H. Karcher proved mathematical existence of Schoens's surfaces whose construction and mathematical existence proof largely could not be understood until 1989.

Using conjugate surfaces and discrete differential geometry bring more surfaces. K. Weirerstrass exhibited simpler examples in this era but they were not widely known for surfaces. In differential geometry, triply periodic minimal surface is a minimal surface in R^3 that is invariant under a rank-3 lattice of translations. Surface elementary shapes vary as rhombohedral, orthorhombic, tetragonal and cubic symmetries. In addition to that, monoclinic and triclinic example existences are known, but it is proven to be very hard to parametrize.

Minimal surfaces were a calculus problem until a NASA physicist, Alan H. Schoen, organized and published the discovered infinite periodic minimal surfaces with self-intersections [16]. After his NASA technical note, minimal surfaces caught attention of people from different areas.

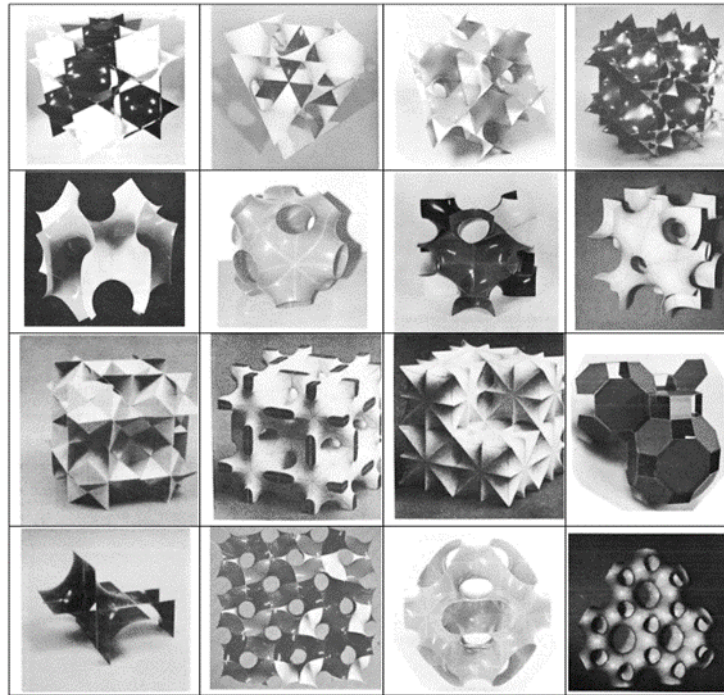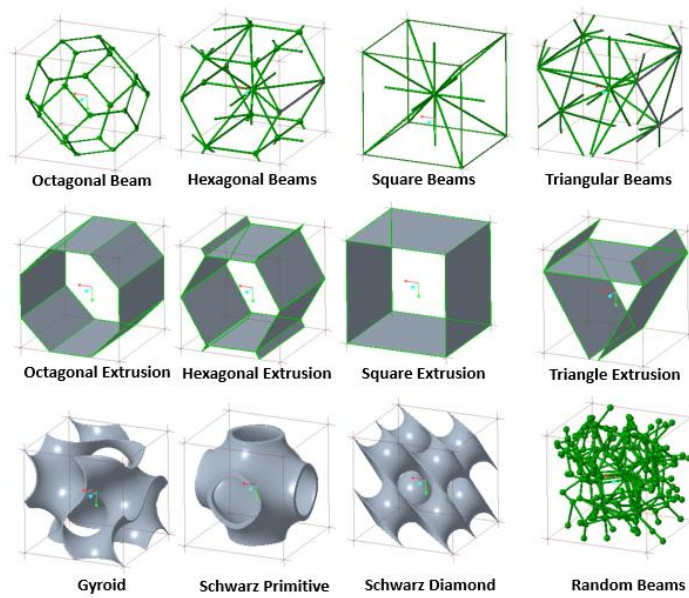*Figure 3.6.* Some Oblique view examples of IPMS from Schoen's Study [16]

Figure 3.7. Most common lattice geometries used in additive manufacturing

42

3.4.1. Selection of Gyroid

All lattice geometries given in Figure 3.7 are investigated during the lattice geometry selection process. All lattices are modelled with the same %15.5 porosity ratio individually and geometric properties such as centroid of volume, total surface area, inertia matrix and principle moments are calculated.

Table 3.1. *Comparison of mechanical properties of various lattice geometries*

Lattice Type	Physical Properties		Centroid of Volume			Princible moments /G		
	Wall Thickness(mm) or Diameter (mm)	Area(mm2)	Gx(mm)	Gy(mm)	Gz(mm)	M1 (gxmm2)	M2 (gxmm2)	M3 (gxmm2)
Triangular Beams	1.3189E+00	1.0029E+03	-3.2927E-07	-1.7665E-01	-4.9484E-07	7.0210E+00	7.3030E+00	7.7190E+00
Square Beams	1.6233E+00	8.6610E+02	2.3318E-01	-5.0000E-06	4.0000E-06	6.9090E+00	7.0270E+00	7.8630E+00
Hexagonal Beams	1.3956E+00	8.6610E+02	2.3318E-01	-5.0000E-06	4.0000E-06	6.9090E+00	7.0270E+00	7.8630E+00
Octagonal Beams	2.0370E+00	6.8139E+02	-7.9118E-08	-4.9648E-07	-2.0000E-06	7.0280E+00	7.0280E+00	7.0280E+00
Triangular Extrusion	5.8493E-01	9.8534E+02	0.0000E+00	-9.5056E-01	0.0000E+00	6.1940E+00	6.7870E+00	7.0280E+00
Square Extrusion	4.8503E-01	1.1501E+03	0.0000E+00	0.0000E+00	0.0000E+00	9.1520E+00	9.1520E+00	1.1870E+01
Hexagonal Extrusion	5.8765E-01	9.7714E+02	0.0000E+00	0.0000E+00	0.0000E+00	7.0680E+00	7.6550E+00	8.2900E+00
Octagonal Extrusion	5.6181E-01	9.9903E+02	0.0000E+00	0.0000E+00	0.0000E+00	8.3300E+00	8.3300E+00	1.0225E+01
Gyroid	6.0000E-01	9.9697E+02	0.0000E+00	0.0000E+00	0.0000E+00	6.3530E+00	6.3800E+00	6.3910E+00
Schwarz P	7.9565E-01	7.5564E+02	8.0000E-06	-2.4400E-04	-3.7000E-05	5.8620E+00	5.8620E+00	5.8620E+00
Schwarz D	7.8205E-01	1.2554E+03	0.0000E+00	0.0000E+00	0.0000E+00	6.8380E+00	6.8380E+00	6.8380E+00

	Inertia Matrix					
	Iox(gxmm2)	Ioy(gxmm2)	Ioz(gxmm2)	Ixy (gxmm2)	Ixz (gxmm2)	Iyz (gxmm2)
Triangular Beams	7.0210E+00	7.7190E+00	7.3030E+00	0.0000E+00	0.0000E+00	0.0000E+00
Square Beams	7.8630E+00	6.9090E+00	7.0270E+00	1.3790E-05	0.0000E+00	0.0000E+00
Hexagonal Beams	7.8630E+00	6.9090E+00	7.0270E+00	1.3790E-05	0.0000E+00	0.0000E+00
Octagonal Beams	7.0280E+00	7.0280E+00	7.0280E+00	0.0000E+00	0.0000E+00	0.0000E+00
Triangular Extrusion	6.1940E+00	7.0280E+00	6.7870E+00	0.0000E+00	0.0000E+00	0.0000E+00
Square Extrusion	9.1520E+00	9.1520E+00	1.1870E+01	0.0000E+00	0.0000E+00	0.0000E+00
Hexagonal Extrusion	7.6550E+00	7.0680E+00	8.2900E+00	8.2900E+00	8.2900E+00	8.2900E+00
Octagonal Extrusion	8.3300E+00	8.3300E+00	1.0225E+01	0.0000E+00	0.0000E+00	0.0000E+00
Gyroid	6.3900E+00	6.3800E+00	6.3530E+00	0.0000E+00	5.4100E-04	4.9920E-04
Schwarz P	5.8630E+00	5.8620E+00	5.8610E+00	2.9730E-04	4.2440E-05	-4.0650E-05
Schwarz D	6.8380E+00	6.8380E+00	6.8380E+00	0.0000E+00	0.0000E+00	0.0000E+00

Although the properties of geometry/matters play important role on selection of lattices, manufacturing the lattice without any support is a critical feature that all lattice should have. Unsupported manufacturing of lattices provides freedom during selection of manufacturing orientation. Therefore, lattice geometries given inFigure 3.9 Figure 3.7 are also manufactured as mock-ups with polylactic Acid plastic material.

Figure 3.8. Manufactured lattice geometries

Figure 3.9. Lattices with interior supports and free support gyroid

Manufactured demo mock-ups show that gyroid geometry is the most suited to implementation as lattice structure due to freedom of orientation during manufacturing.

3.4.2. Gyroid IPMS

The gyroid is one of the famous infinitely periodic minimal surfaces. It is very commonly used in plastic 3d modelling. It is one of its kind, non-trivial embedded member of the associate family of the Schwarz P and D surfaces with association approximately 38.01° with respect to each other.

The gyroid is like the lidinoid and discovered by Schoen [16]. He calculated the angle of association and gave a convincing demonstration of plastic and paper models, but did not provide a proof of embeddedness.
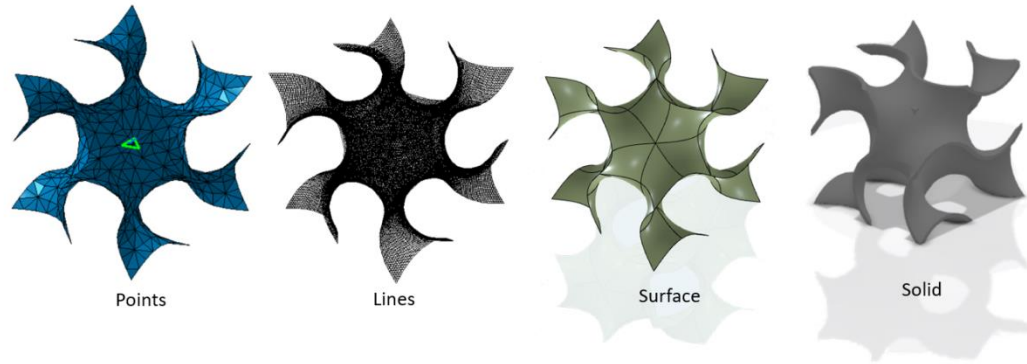
Figure 3.10. Gyroid Surface (Appendix B)

The gyroid surface can be trigonometrically expressed as:

$$\sin(x)\cos(y) + \sin(y)\cos(z) + \sin(z)\cos(x) = 0 \qquad (3\text{-}37)$$

It does not contain straight lines and planar symmetries, it is curly and periodic
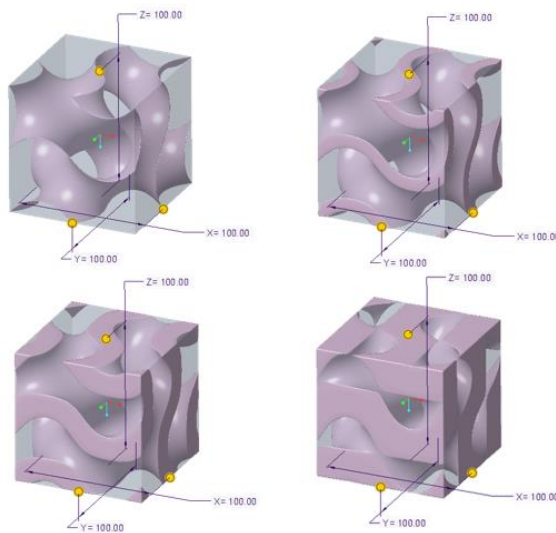
Figure 3.11. Gyroid geometry with different symmetrical thickness variations

3.4.2.1. Simplified Gyroid Structures

Lattice structures bring many problems in practice. The smaller lattice structures become, the more model data it will have. Minimal surfaces are very detailed and complicated surfaces. Single lattice include more than 100 nodes and single structural part includes thousands of lattices. This brings memory and CPU problems during modelling of the structural part.

S.N. Khaderi, V.S. Deshpande, N.A. Fleck, [33] simplified the gyroid structure with beams in their article to decrease model data during modelling lattice structural mechanical parts. Figure 3.12 and Figure 3.13 show the orientation of each beam in 2D and 3D.
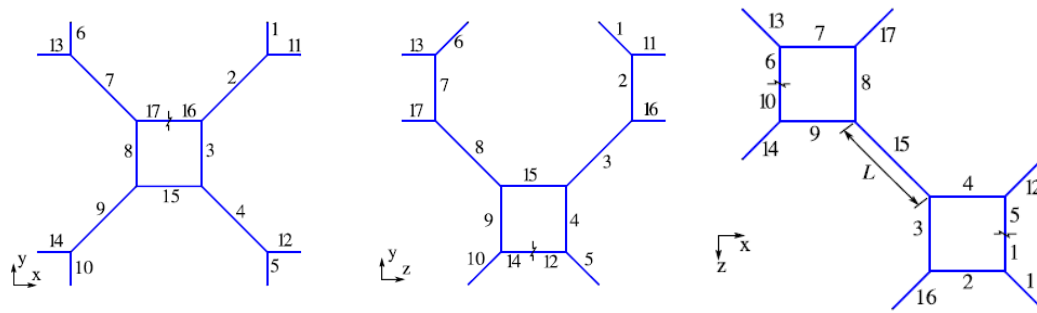
Figure 3.12. 2D Orientation of each beam in cell [11]
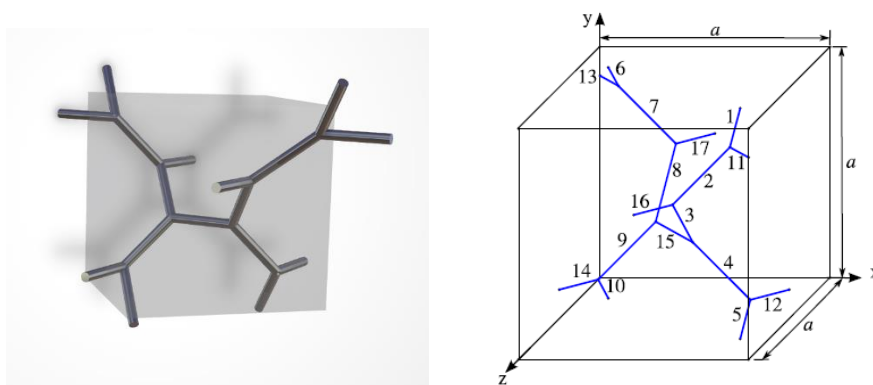
Figure 3.13. 3D Orientation of each beam in cell [11]

In addition to beam simplification, helix geometry also has many similarities with simplified beam structure. If interval distance and pitch matched, it can also be simplified with helix geometries.

|(a)|(b)|
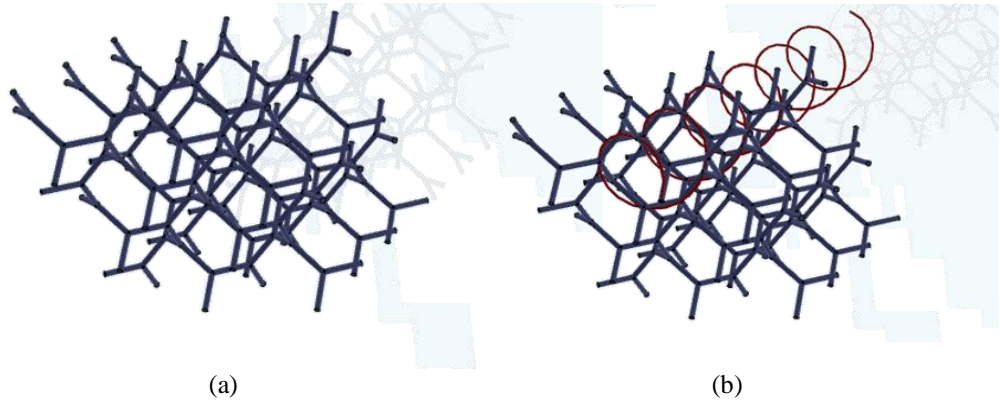
Figure 3.14. a- Simplified gyroid structure with beams   b- Helix Conversion of simplified gyroid Structure
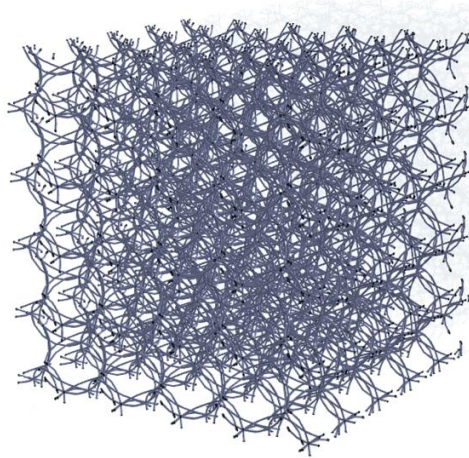
Figure 3.15. Simple cube structure created with helix geometries

However, studies show that even helix and beams simplify the geometry, they do not provide major advantages during modelling of structural parts. This simplification will not be applied in this thesis work.

3.5. Minimal Surfaces with Additive Manufacturing

Bidirectional-offset-union strategy in two-dimensional space gives capability to create layered infill areas for fabricating solid triply periodic minimal surfaces with uniform wall thickness. This proposed strategy is robust and reliable for both open and close slicing contours.
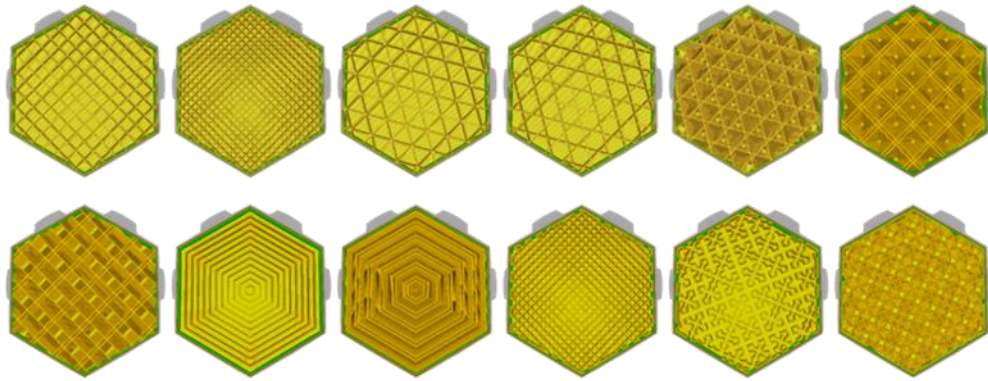
Figure 3.16. General infill patterns that is used in Plastic 3D printers [14]

Infill geometries are very popular in plastic 3D printing and changes with respect to many perspectives. On the other hand, cellular lattices take infill's place in metal 3D printing. Some examples of metal 3D printing shown in Figure 3.17.

(a) P surface   (b) G surface   (c) D surface   (d) I-WP surface

(e) Manufacturing with generated layered infill areas
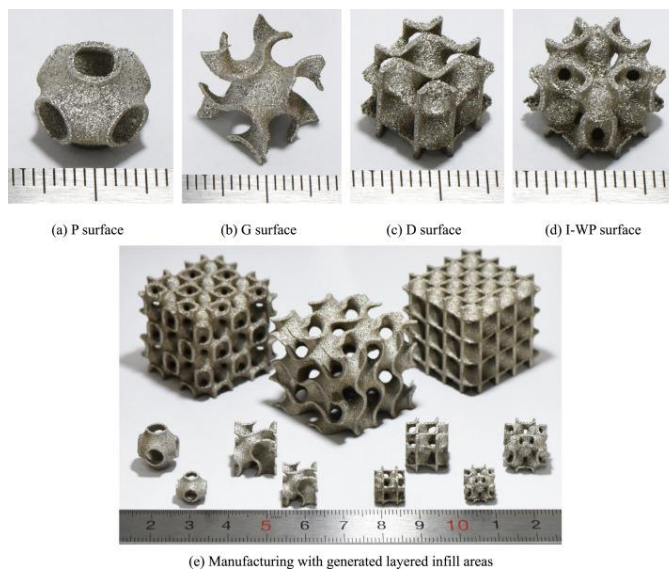
Figure 3.17. IPMS surfaces with AM [9]

CHAPTER 4

CASE STUDY & OPTIMIZATION OF A/C PART

4.1. Aircraft Boarding Step as a Case Study

Boarding step is the first and last thing a pilot will experience of his/her flight. The system is designed to board pilot easily to the aircraft. It is one of the systems need to satisfy unique requirements. Its location is determined with the limits of human body and its volume is limited to satisfy enough space for pilot foot area given by human machine interface (HMI) relying on MIL-STD-1472 "human engineering design criteria for military systems, equipment and facilities" standard.

Boarding system can be placed in both externally and internally. External boarding steps are classified as ground support units. After the landing, they are placed by technicians. They provide the advantage of comfort and no additional system weight on aircraft. However, they require additional human labor on the ground.

Figure 4.1. Boarding step designs of the F-35   (Photo: Lockheed Martin)

On the other hand, internal boarding steps are generally used for military applications. They are designed for rough, war conditions where qualified technicians/human labor are limited. They eliminate requirement of ground support and shorten flight preparation time. They are only used two times per flight and carried during all operations. Thus, reducing the system weight increases aircraft efficiency.

Figure 4.2. An example of boarding step without/with body fairing on aircraft

An example of slider boarding step design is shown in Figure 4.2. Its extended position is shown in first two pictures and it is retracted into wing body fairing during flight to increase aerodynamics and efficiency.
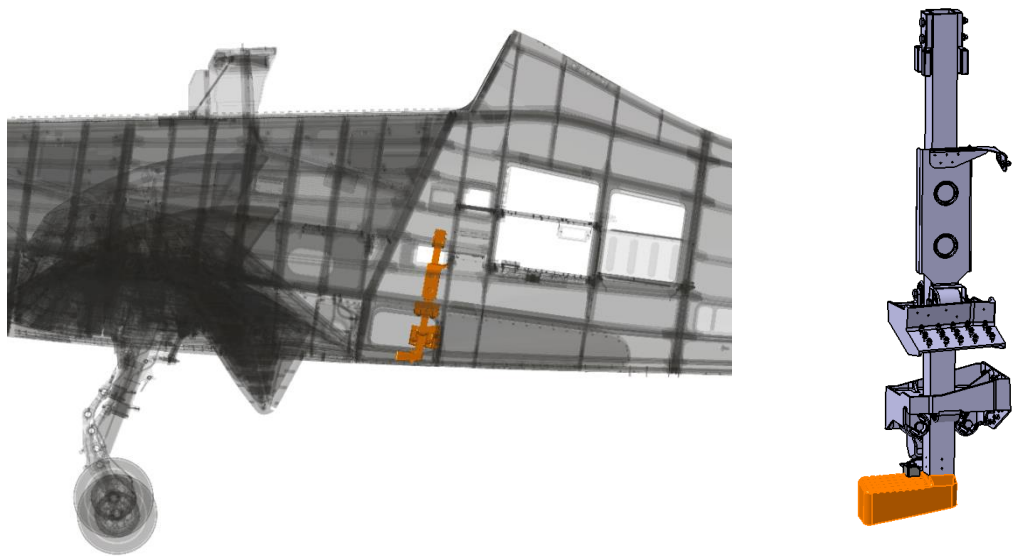
Figure 4.3. CAD model of boarding step mechanism and its position on aircraft
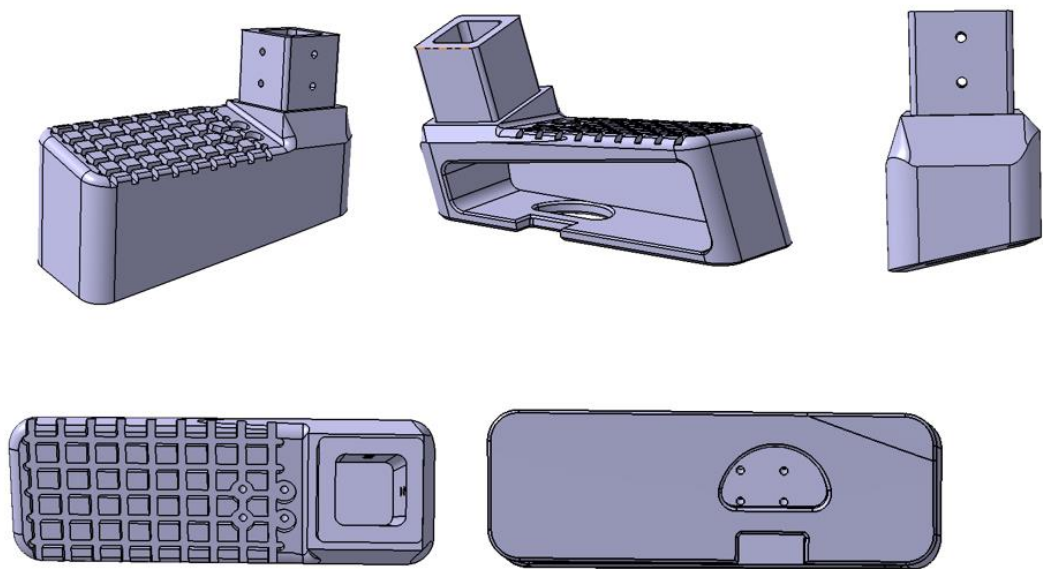
Figure 4.4. Detail view of footstep

4.2. Determination of Flight Loads on Footstep

Finite element model is implemented as master model between two frames of aircraft in Fig. 5.5 where boarding step is positioned. The flight loads are taken from civil aircraft standards CS23.
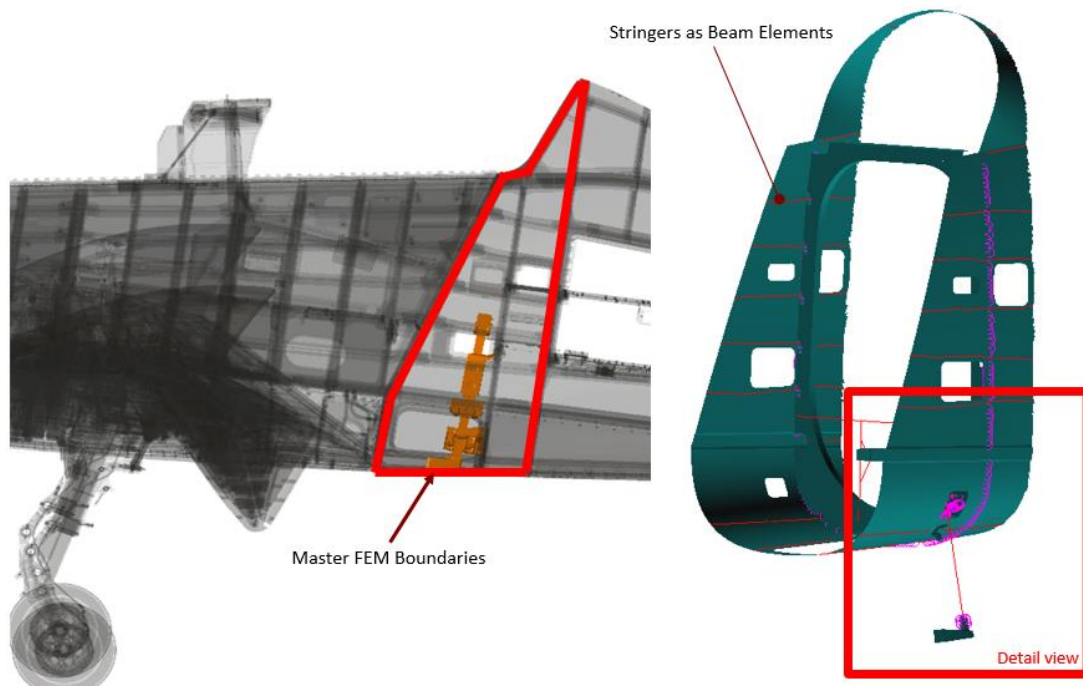
Figure 4.5. FEM model of boarding step (two frame section is modelled)

Detail view of the boarding step finite element model is shown below in Figure 4.6. The connections between the fittings are simulated with fastening connection. The constant cross section elements such as boarding step beam is modelled as 1D rigid element, shown as red line in Figure 4.6, and it is connected to boarding step with fastener connection.
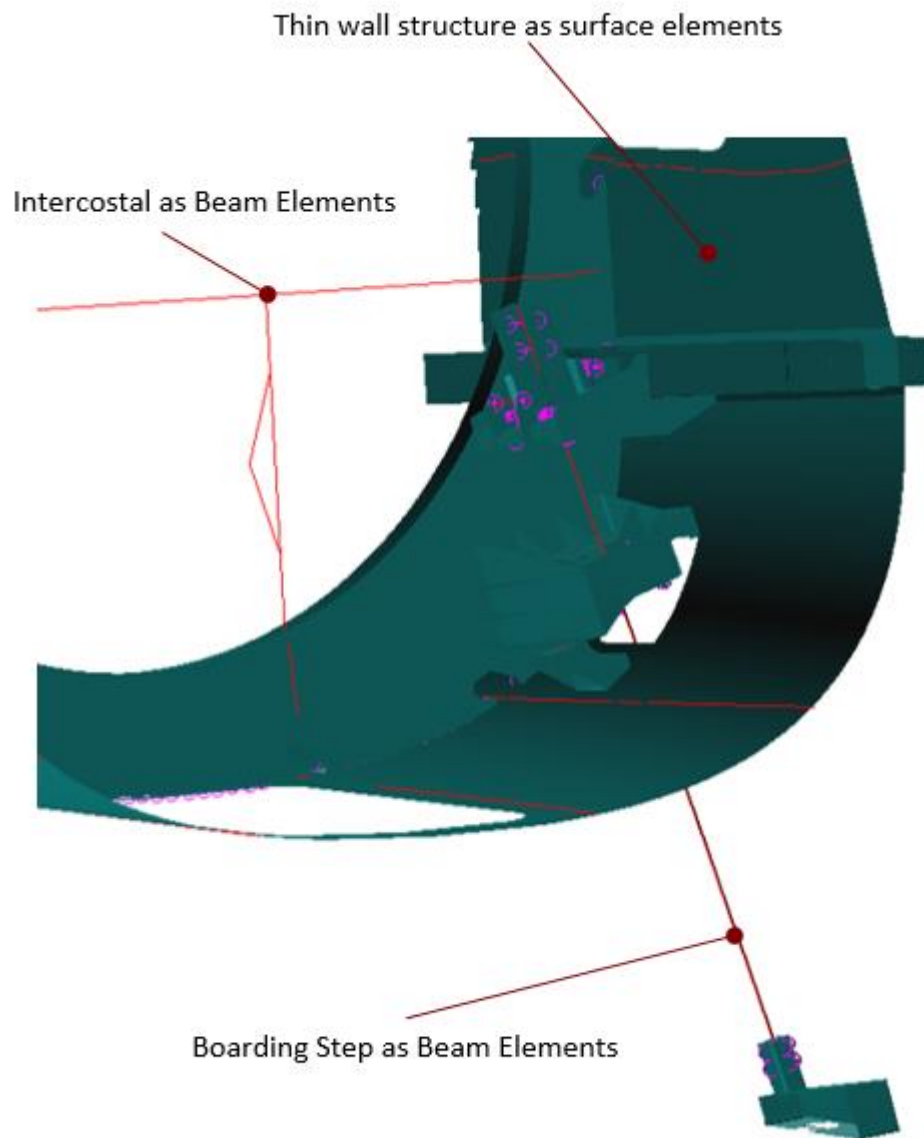
Figure 4.6. Detail view of master FEM model

Four loads which are limit and ultimate flight loads, emergency landing loads and inertia load envelope are taken into consideration as load cases applied on boarding step mechanism.

Table 4.1. *Load cases implemented on boarding step*

	Flight Loads (Limit)			Emergency Landing Loads	
N_x	2.4g	(Backward)	N_x		(Backward)
	-0.5g	(Forward)		-13.6g	(Forward)
N_y	3g	(Left)	N_y	2.27g	(Left)
	-3g	(Right)		-2.27g	(Right)
N_z	11g	(Downward)	N_z	9.1g	(Downward)
	-5.5g	(Upward)		-5g	(Upward)
	Flight Loads (Ultimate)			Maximum Inertia Envelope	
N_x	3.6g	(Backward)	N_x	3.6g	(Backward)
	-0.75g	(Forward)		-13.6g	(Forward)
N_y	4.5g	(Left)	N_y	4.5g	(Left)
	-4.5g	(Right)		-4.5g	(Right)
N_z	16.5g	(Downward)	N_z	16.5g	(Downward)
	-8.25g	(Upward)		-8.25g	(Upward)

In addition to flight loads, pilot weight is also defined as load case during the boarding procedure. The standard human pilot weight is taken as 124kg with safety factor of 1.3 that results in 1581N limit and 2372N ultimate load applied vertically on the step. This is taken as a static load case of the boarding step. Static case solution can be seen below.
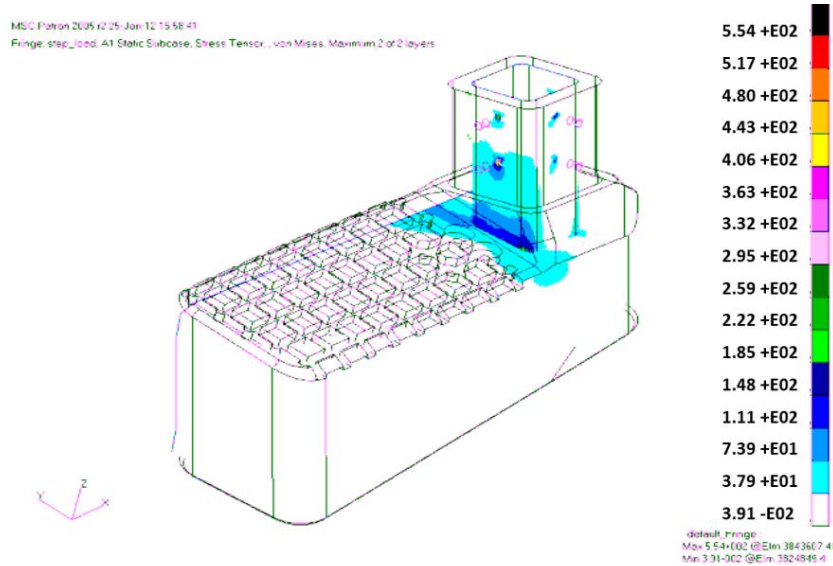
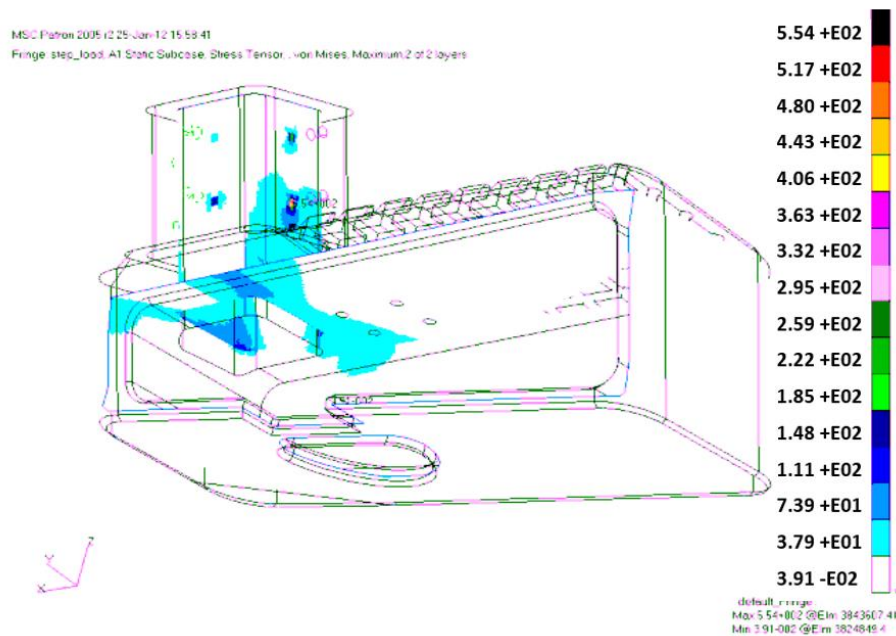*Figure 4.7.* FEM result of boarding step in Nastran (isometric view)

Figure 4.8. FEM result of boarding step in Nastran (side view)

Analysis shows that boarding load (pilot weight) dominates all load cases. Flight and emergency landing load cases are nearly negligible due to high mechanical properties of the boarding step material, a titanium alloy. Dominant loads can be seen on
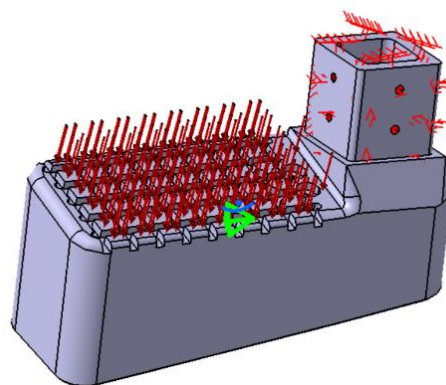
Figure 4.*9*.

Figure 4.9. Dominant load directions and constrains

4.3. Validation of Finite Element Solver before Topology Analysis

Catia is one of the most common used CAD softwares in defense industry. It does not only help to model any product but also it has many features that support designers during designing, analyzing, manufacturing and simulation processes.

Catia FEA Static case provides three different solution options to users with two gradient parameters which are "maximum iteration number" and "accuracy". Loads, Constrains, Material properties are implemented directly into the model and solved with FEA. The solution options can be described as follows:

- *Gauss:* It is a direct method used in the computation of small/medium models. The stress is computed at the Gauss points. Displacements are calculated at the nodes. All other displacements are interpolated from the shape functions.
- *Gauss R6:* It is a fast Gauss method that is used in the computation of large models.
- *Gradient:* It is an iterative method that is used for huge models. It saves memory but it requires too much CPU time. However if the model contains contact elements generally Gauss R6 is used for better results.

Thick beam problem and beam bending problems are used to validate Catia FEA module.In the Thick beam problem, one edge is constrained with respect to T_x and T_y and force is implemented to the other edge of a 2D beam. The analytical solution for Case1 and Case 2 calculated as $T_y = 100.00$mm and $T_y = 102.60$mm. The FE solution is performed using the following parameters:
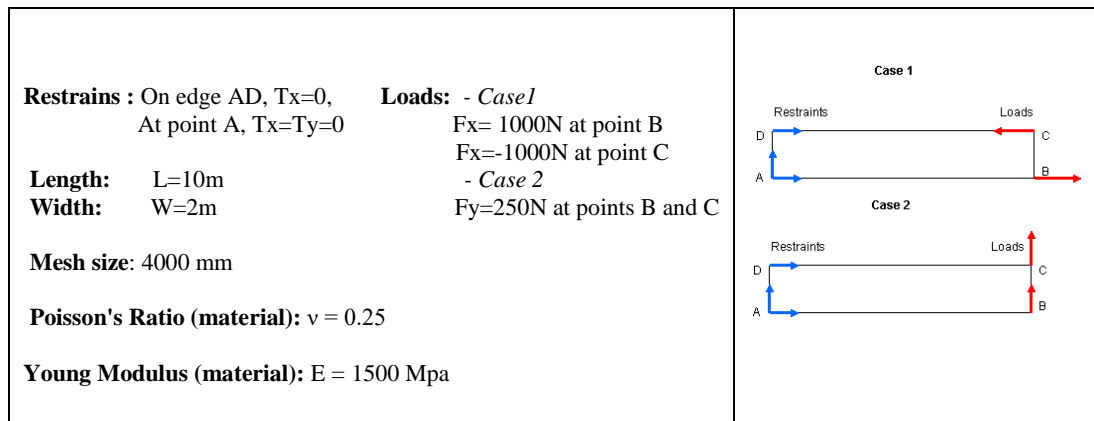
Figure 4.10. Thick Beam Problem Definition

FEA results with respect to mesh shapes are shown in the following:

	Analytical solution [mm]	Values							
		Linear triangle (TR3)		Parabolic triangle (TR6)		Linear quadrangle (QD4)		Parabolic quadrangle (QD8)	
		Computed results [mm]	Normalized results	Computed results [mm]	Normalized results	Computed results [mm]	Normalized results	Computed results [mm]	Normalized results
Case 1	100	25.49	0.255	100	1.000	96.18	0.962	100	1.000
Case 2	102.6	29.78	0.290	101.54	0.989	98.05	0.956	102.8	1.002

Figure 4.11. Results for different Finite Element Shapes[19]

In the beam-bending problem, one edge is translation with respect to all axis and rotation on z-axis is constrained. Bending moment is applied on point C. The material properties such as young modulus and poisson's ratio and geometrical dimensions of the beam is given on Figure 4.12.
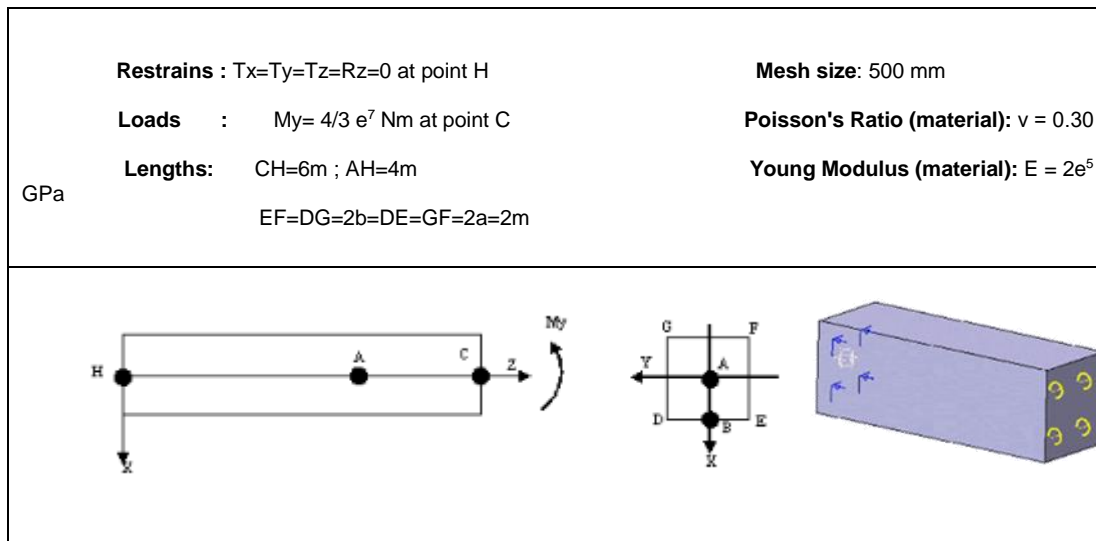
Figure 4.12. Beam Bending Problem Definition

Figure 4.13. Results for different Finite Element Shapes[15]

Catia FEA module provides %96 (worst case) accuracy for 2D calculations for all element types and provides %99 accuracy if TE10, HEB and HE20 elements are selected for 3D model. The results show that Catia v6 module is very reliable if the correct mesh size and type are chosen for the problem.

4.4. Determination of Load Carrying Elements with SIMP Method

4.4.1. Finite Element model and optimization parameters

Four different load cases are applied to finite element analysis and worst case stresses are investigated on the boarding step.

Four flat sides of fitting are defined as contact surfaces. Eight fastener connection points are fixed in 6 DOF and model is created by TET10 solid elements. SIMP method is applied to determine main load carrying elements.

While thinking free body diagram of the boarding step, it is assumed that only the upper connections, 8 rivets, are fixed in 6 DOF and pilot weight 2372N is applied to step on –Z direction.
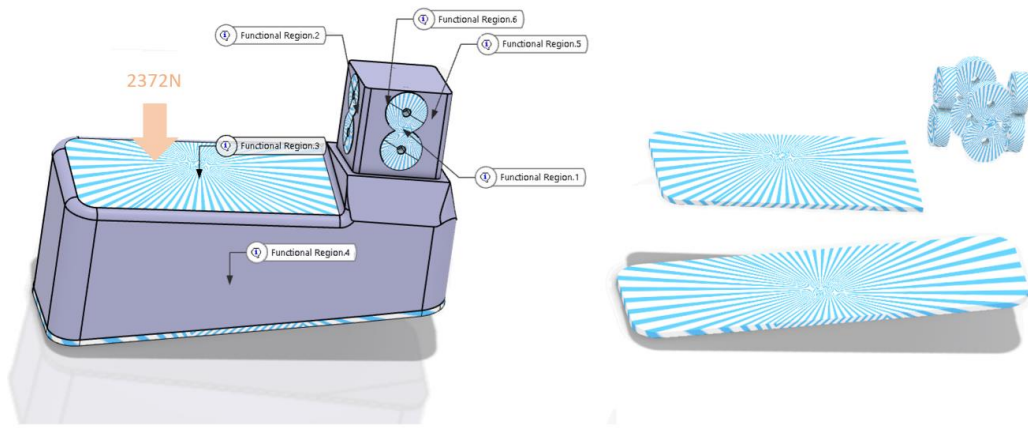

Figure 4.14. Functional regions

Six functional regions are defined on the design domain. Functional region 1,2,5,6 is defined as solid for rivet connections. Load case is defined on functional region 3 and functional region 4 is also defined solid to keep aircraft surface continuous.

The model for the topology optimization is modified in such a way that the inner areas of the component are filled with elements to create a design area where the optimization system can remove or rearrange elements for getting a better mechanical behavior of a component with a lower weight and with the same mechanical behavior.

Table 4.2. *Optimization parameters*

Object Function	Number of iterations	Target Mass	Element Size
Minimum Compliance	50	%20	0.5mm

Minimum member size can easily be implemented in the finite element model. The minimum size of the elements is generally driven by manufacturing capabilities. Increasing the resolution of finite element model increases the resolution of the resultant geometry. However, it also increases computational cost of the problem. 1 mm element size is the general trend in most of the applications. 1.5 mm minimum member size is a feasible starting point when taking into consideration the roughness of electron beam melting part's surfaces. It is recommended that minimum member size should be at least three times larger than the finite element size that drives to minimum element size to 0.5mm.

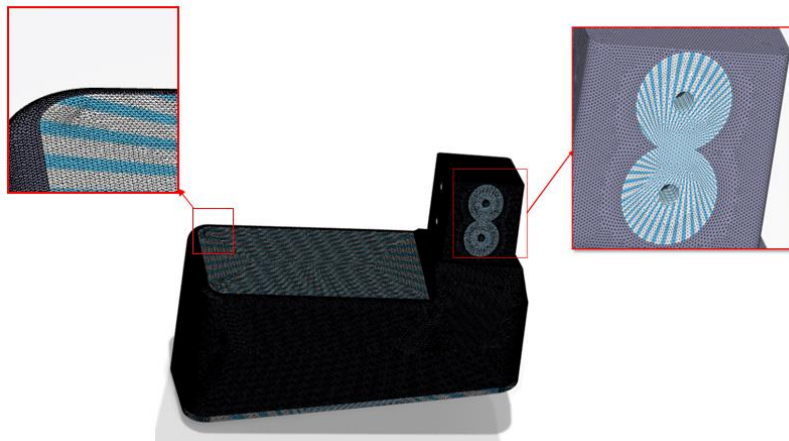*Figure 4.15.* Generated mesh on footstep

4.4.2. Optimization results

By using function driven generative design module in Catia, the optimization is performed. Material density plot that shows the material densities between 0 and 1 is shown in Figure 4.16. The SIMP method gives the artificial densities (pseudo densities) of each element at the iteration 50. Density=1 defines %100 effective

elements and density=0 gives %0 effective elements. Density distribution through design volume also gives the distribution of load carrying elements.
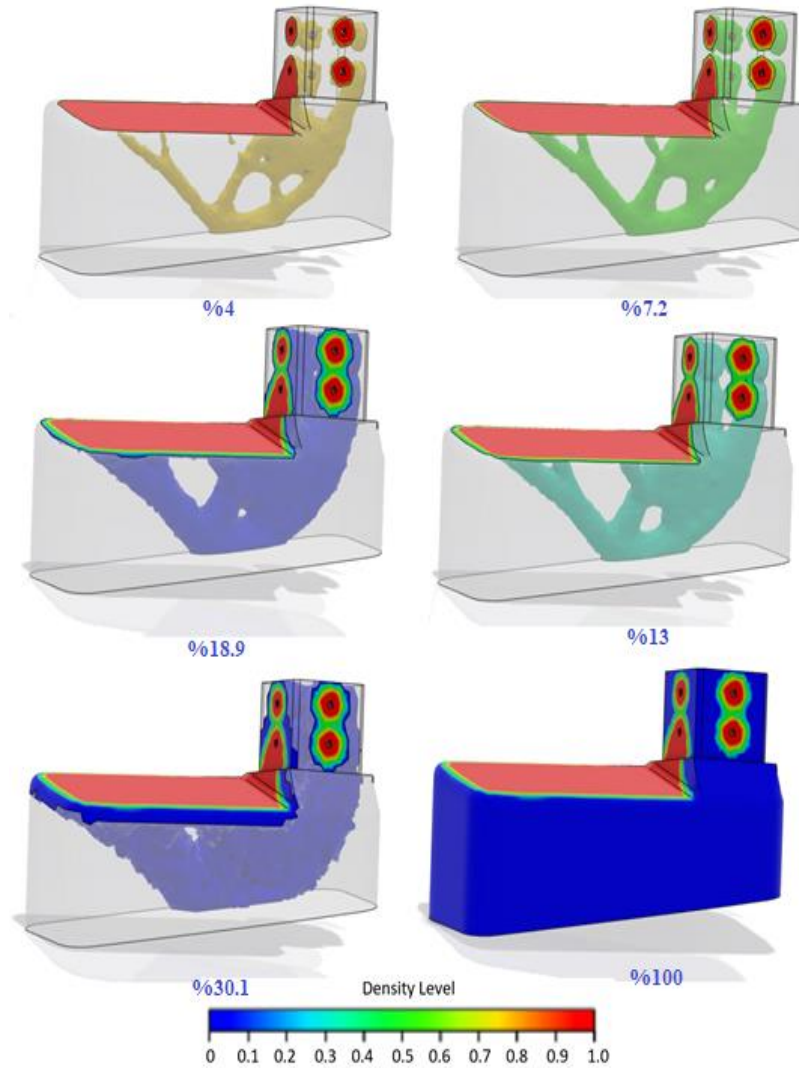
Figure 4.16. Main load carrying elements. Residual volumes are %4, %7.2, %13, %18.9, %30.1 and %100 from left to right/above to below

Result clearly shows that the load carrying elements are positioned on very close to constrained holes and distributed zone surface. Moreover, lower structure branches to prevent bending moment at the end of the footstep. Stiffness and mass variations of each iteration are shown in Figure 4.17 and Figure 4.18.
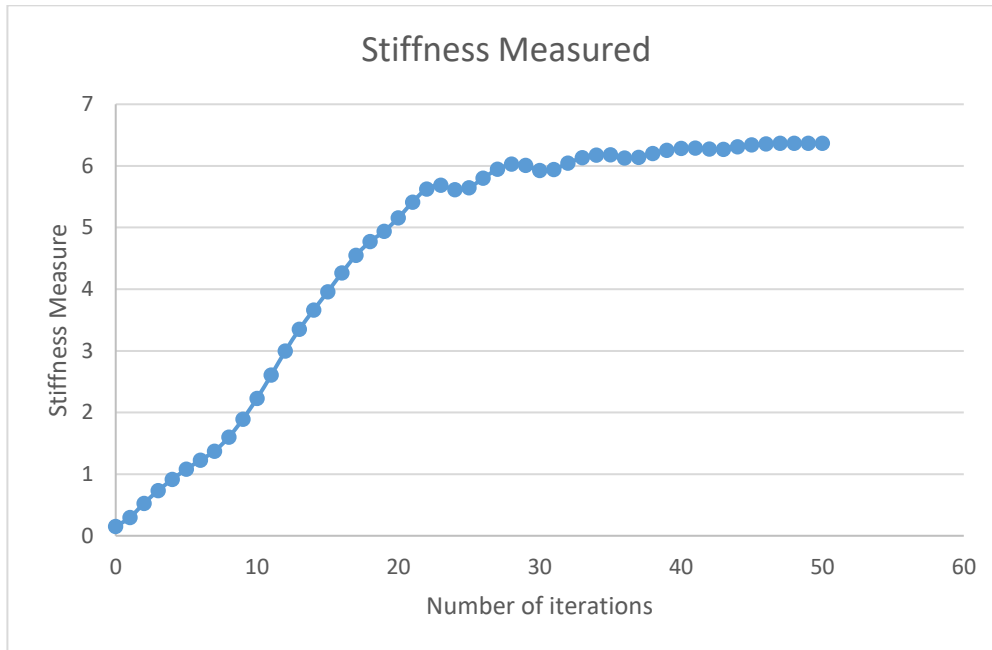
Figure 4.17. Stiffness change during iterations
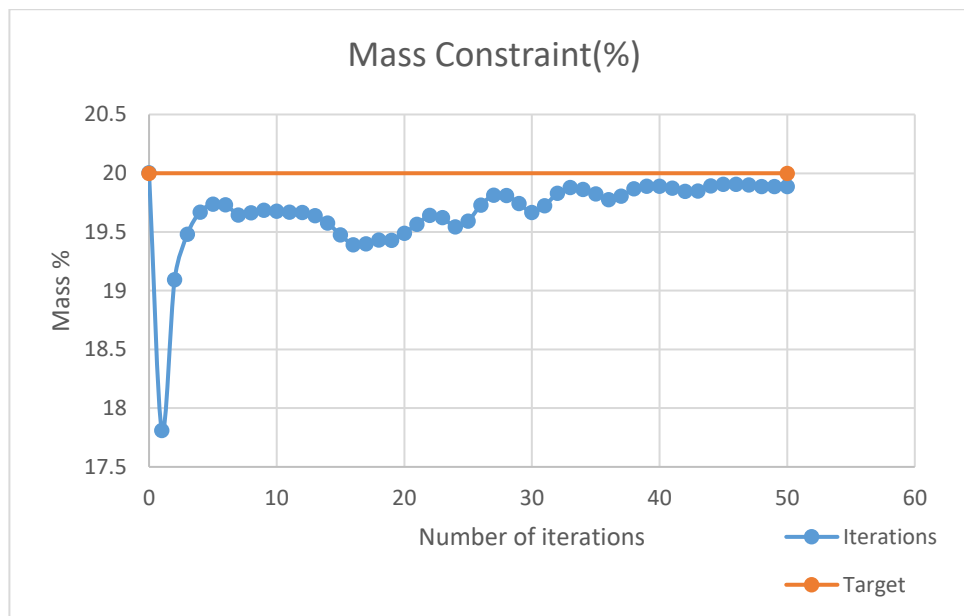
Figure 4.18. Mass variations during iterations

4.5. Combining Load Patterns with Lattices

Even the load density levels are created, the resultant geometry is very rough and need smoothing operation for manufacturability and operational limitations. The resultant geometries are smoothed to ensure the continuity of the surface tangency.

Figure 4.19. Main load carrying elements after smoothing operation. Residual volumes are %4, %7.2, %13, %18.9, %30.1 and %100 from left to right; above to below

Residual Volume %4
Residual Volume %7.2
Residual Volume %13
Residual Volume %18.9
Residual Volume %18.9
Residual Volume %100

Figure 4.20. Mid-Section view of load boundary surfaces

Gyroid is a surface element and thickness of the lattice can be varied in the design process. Required mechanical stiffness can 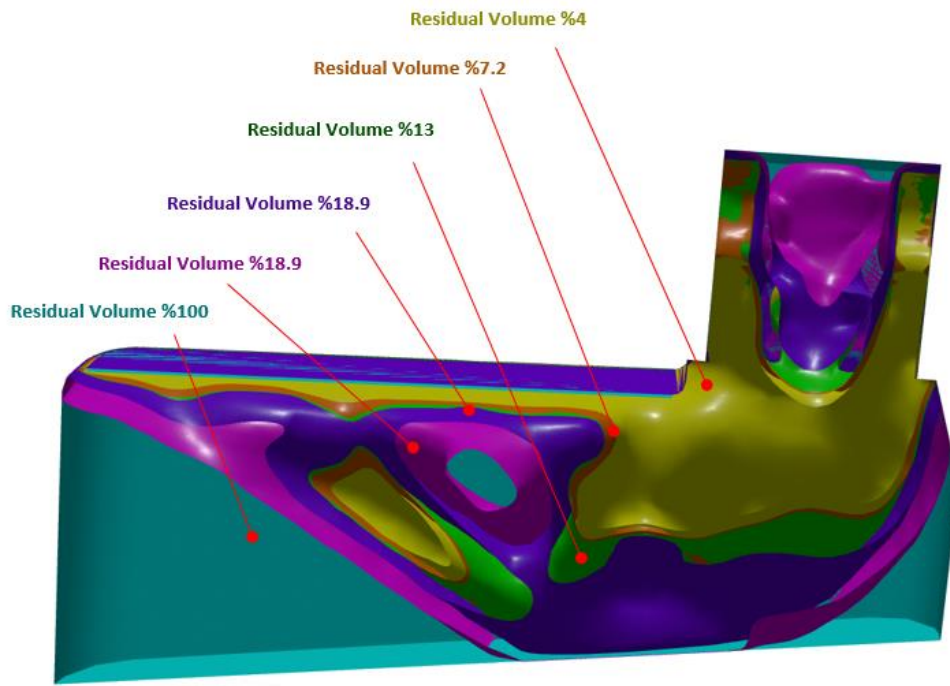be provided by thicker lattice with lover residual volume or thinner lattice with higher residual volume. On the other hand, higher residual volume brings more stiffness due to increase in inertia. As a result of this, lowest thickness value which is 0.6mm that electron beam melting can produce is selected and residual volume is increased until the stress constraint is satisfied. It is shown that residual volume %7.8 is very close to provide 539 Mpa stress constraint that gives 1.54 RF with lowest yield value 831 Mpa from previous studies.

The lattice pattern is divided into two main geometries. The blue lattice pattern carries the load and satisfy the stress constraint, green lattice pattern infills between structure and the outer boundary. Boundary shell of inner lattice is implemented as 0.6 mm thickness to prevent unexpected stress concentrations. Surroundings of rivets with distance 7.4 mm (2*diameter+1) are kept as full solid geometry that is left around

64

fastening holes to prevent bearing and solid covering surfaces. The lattice boundaries for this two-pattern cam ne seem on Figure 4.21.Note that all other elements are hidden to clear the visibility of the lattices.

Figure 4.21. Gyroid lattice patterns on boarding step

It is shown that using lattices for boarding step can cause sharp edges on endings. The sharp free edges of lattices are covered with 0.2 mm of shell surfaces to improve part stiffness and manufacturability.
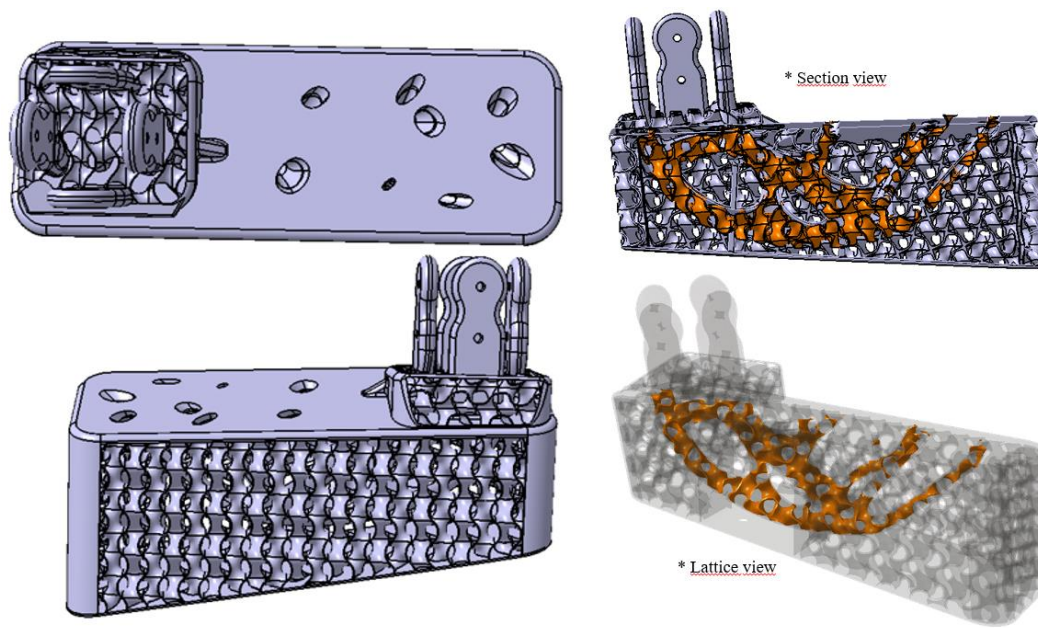
Figure 4.22. Final geometry

The resultant geometry includes very thin and thick parts at the same time thus usage of constant element size is not cost effective with respect to computational time. Mesh is generated in iterative process to provide %4.3 global error. The mesh is constructed by adaptive mesh tool of Catia FEA with the limits of 0.2mm and 1mm. Nearly 460.000 element is constructed and %4.3 global error is achieved. The geometry is formed as low resolution around shell surfaces and high resolution around load carrying lattices and connection points. The mesh geometry is shown in Figure 4.23.

Figure 4.23. FEM model of optimized model with lattice structure

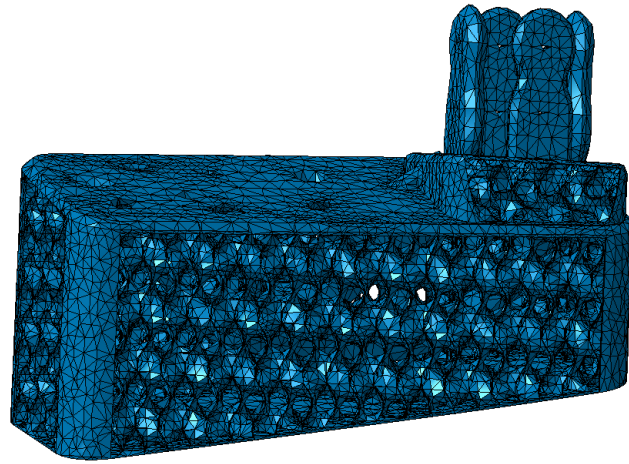FEA Analysis is performed with optimized model. The stress is concentrated around bending corner that is between the connection points and the force plane as expected. Von Mises stress distribution plot is shown in Figure 4.24.
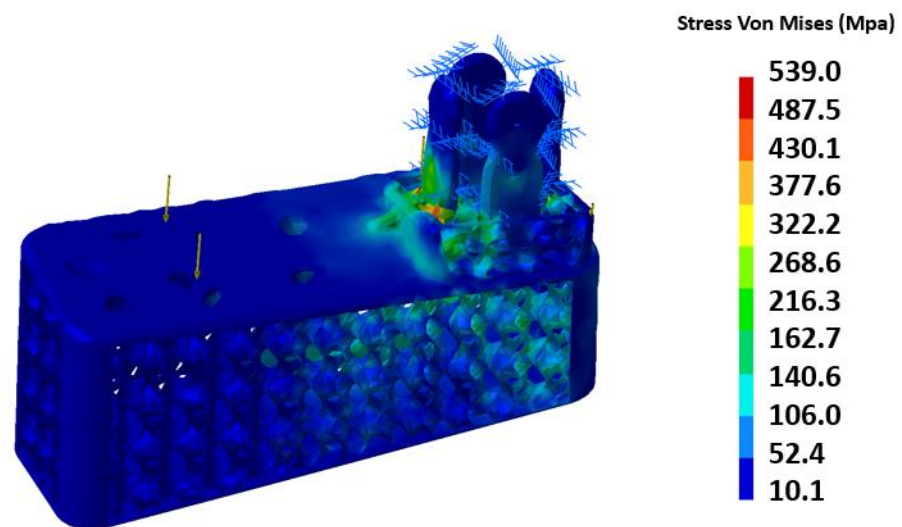
Figure 4.24. Von mises stress distribution plot

Detailed view of inner lattice Von Mises stress distribution plot is shown in Figure 4.25. It clearly shows that inner lattice carries the load as expected.
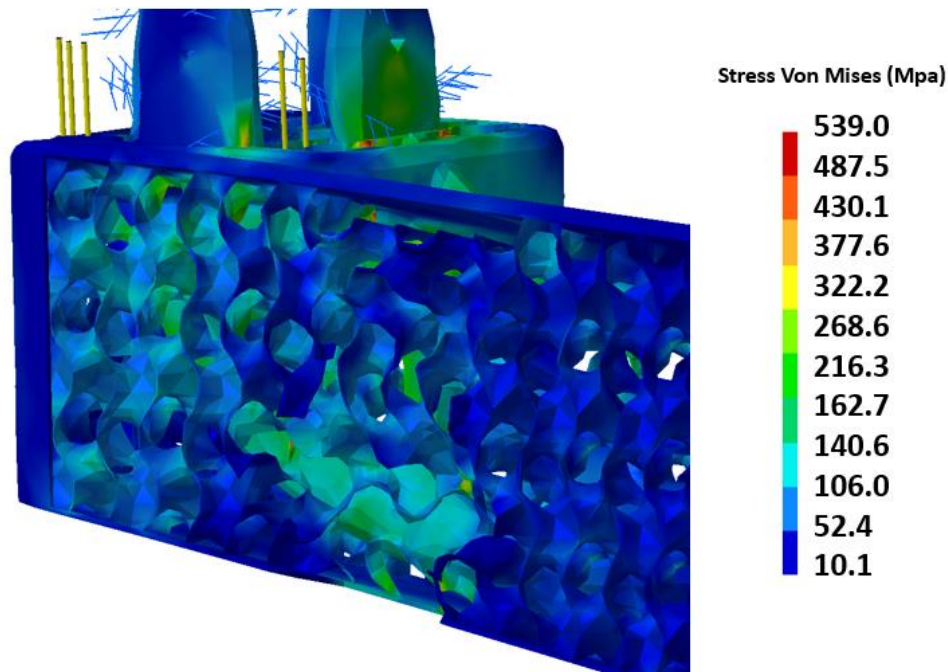
Figure 4.25. Load carrying inner lattice in detail

Overall, static analysis result is shown in Table 4.3

Table 4.3. *FE results*

Max. Von Mises Stress	*RF*	*Max. Displacement*
539 Mpa	1.54	2.72×10^{-2} mm

4.6. Pre Manufacturing/ Producibility Checks

Plastic materials are also widely used in additive manufacturing. They are very cheap and easy to implement in a component. Polylactic Acid (PLA) printers are excellent

examples to simulate support structures for manufacturing. Mock-up of final geometry was manufactured with PLA and there were no conflicts during manufacturing.
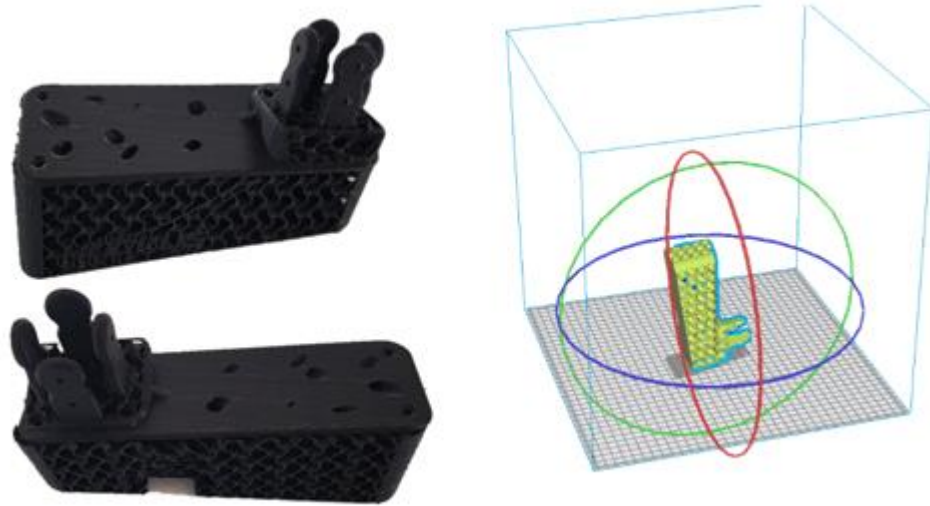
Figure 4.26. Mock-up of final geometry built with PLA

4.7. Topology Optimization without Lattice

Implementation of lattice structure in optimization process is one of the main aims of this thesis. However, topology optimization without lattice with materials, 7050 T7451 Aluminum and titanium Ti6Al4V is performed to see effects of lattice implementation and material properties on topology optimization. Totally, the same procedure is followed except lattice implementation. The geometry that is created by SIMP method only smoothed and directly implemented to the design.

Titanium Study

Optimization parameters are as the following:

Object Function:	Minimum compliance
Target Mass:	%20 of design volume
Max number of Iteration:	50
Material:	Ti6Al4V
Stress Constraint:	540 Mpa (for RF=1.54)
Load Case:	2372N (-Z direction)

The optimization process has reached the target mass in 48 iteration. The stress constraint will be provided with resultant %6.8 residual volume. The overall geometry of resultant optimized geometry is shown in following Figure 4.27 below:
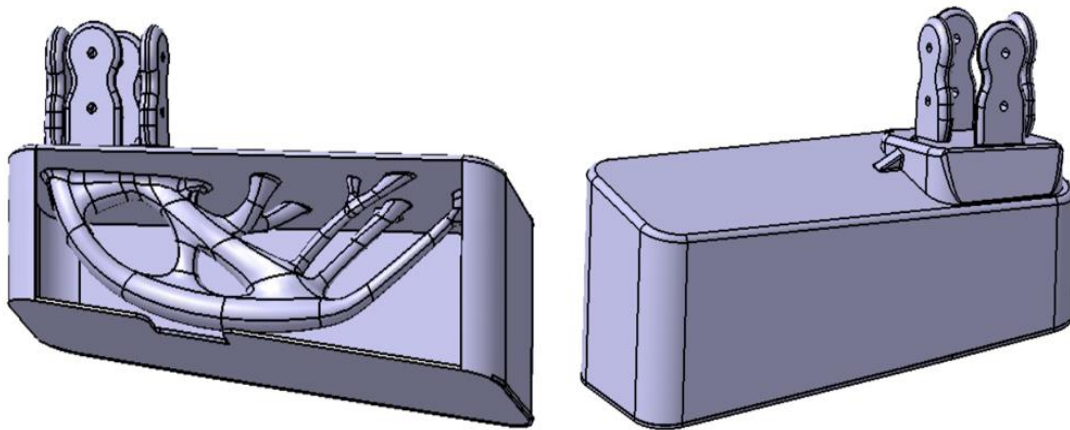

Figure 4.27. Optimized geometry with Ti6Al4V material without lattice structures

Finite element mesh and analysis results are shown in Figure 4.27.The results show that the mass of the final geometry is heavier because of %100 fulfillment rate when compared to lattice geometry even it has a lower residual volume.

Figure 4.28. Mesh and FEA results of Ti6Al4V design

The resultant geometry has 284gr weight, 64cm^3 volume. The maximum displacement on load case is 0.13mm at the tip of the boarding step. The optimized geometry is 40gr heavier when compared to optimized lattice geometry.

Aluminum Study

Optimization parameters are as the following:

Object Function:	Minimum compliance
Target Mass:	%20 of design volume
Max number of Iteration:	50
Stress Constraint:	305 Mpa (for RF=1.54)
Material:	AL7050 T7451
Load Case:	2372N (-Z direction)

The optimization process has reached the target mass in 50 iteration. Aluminum 7050 T7451 has a yield strength of 469Mpa. As a result of this, stress constrain determined as 305 Mpa. The stress constraint will be provided with resultant %10.7 residual volume. The overall geometry of resultant optimized geometry is shown in Figure 4.29.
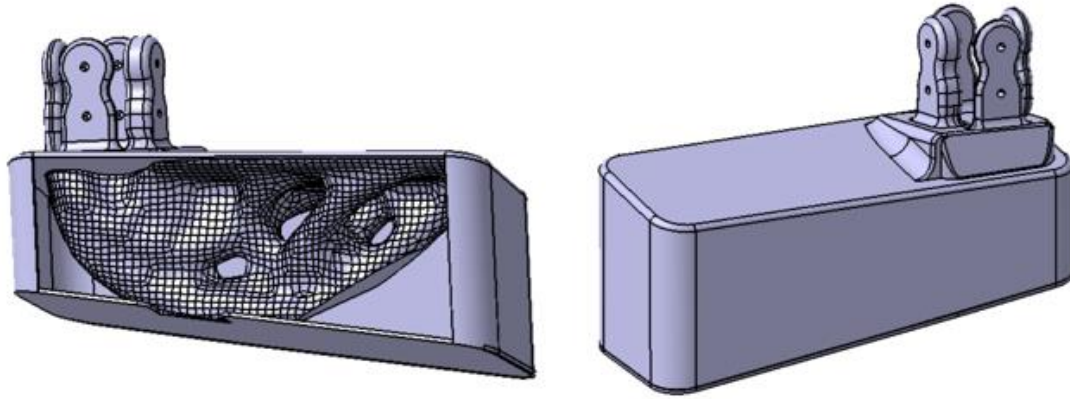
Figure 4.29. Optimized geometry with AL7050 T7451 material without lattice structures

Validation FEA is performed to map stress distribution over the resultant geometry of aluminum design. The results shows that the most critical regions are the connection corners that exposed to bending moment due to space limitations on that region.
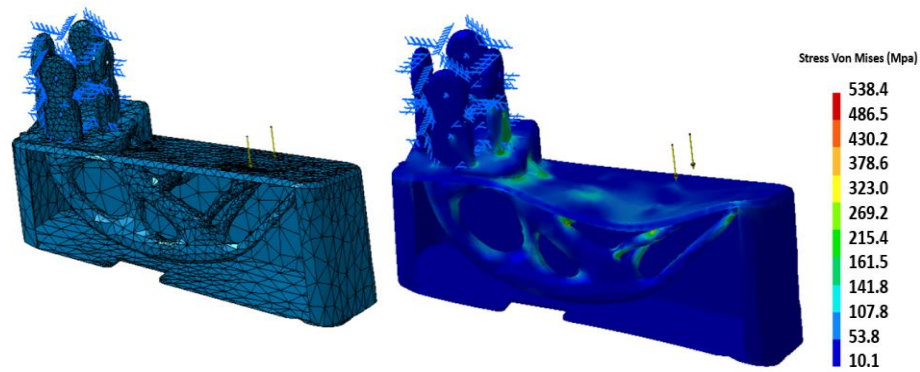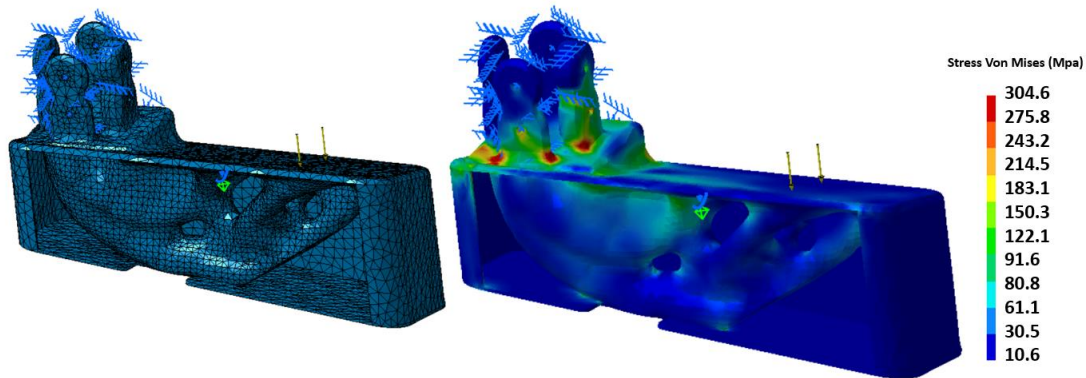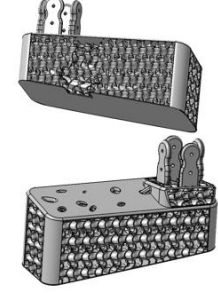

Figure 4.30. Mesh and FEA results of AL7050 T7451 design

The resultant geometry has 263gr weight, 97cm^3 volume. The maximum displacement on load case is 0.08mm at the tip of the boarding step. The optimized geometry is 40gr heavier when compared to optimized lattice geometry.

Table 4.4. *Comparison of optimized geometries*

	New Topology Optimizated Aluminum Design	New Topology Optimized Titanium Design	New Lattice Design
Material	AL7050 T7451	Ti-6Al-4V	Ti-6Al-4V
Weight	263gr	284gr	243gr
Material Volume	97.052 cm^3	64.130 cm^3	52.710 cm^3
Displacements	0.082mm	0.138mm	0.027mm
Reserve Factor	1.54	1.54	1.54

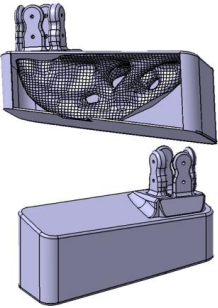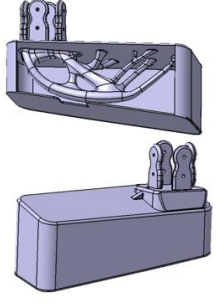Results shows that low-density low strength aluminum (AL7050 T7451) provides more profit when compared to high-density high strength titanium (Ti6Al4V) due to stiffness gain from higher residual volume. On the other hand, lattice structure provide best results spread through all design space. The comparison study clearly shows that increasing design space is more beneficial for lighter designs if there is no concentrated load and tough design space limitations.

4.8. Comparison of Existing Designs

Two previous concept design studies for boarding step, conventional aluminum design and 3D woven composite design, are already manufactured. It has a unique feature that has the capability to compare design studies using different materials.
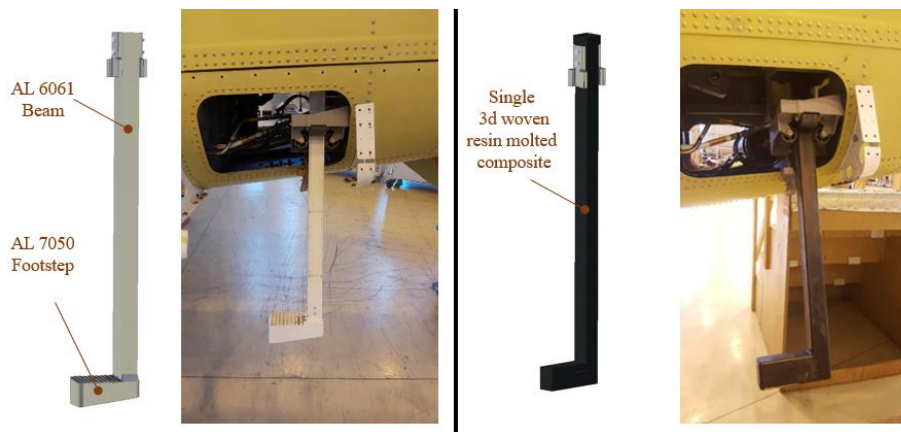
Figure 4.31. Existing aluminum and 3d woven boarding step designs on aircraft
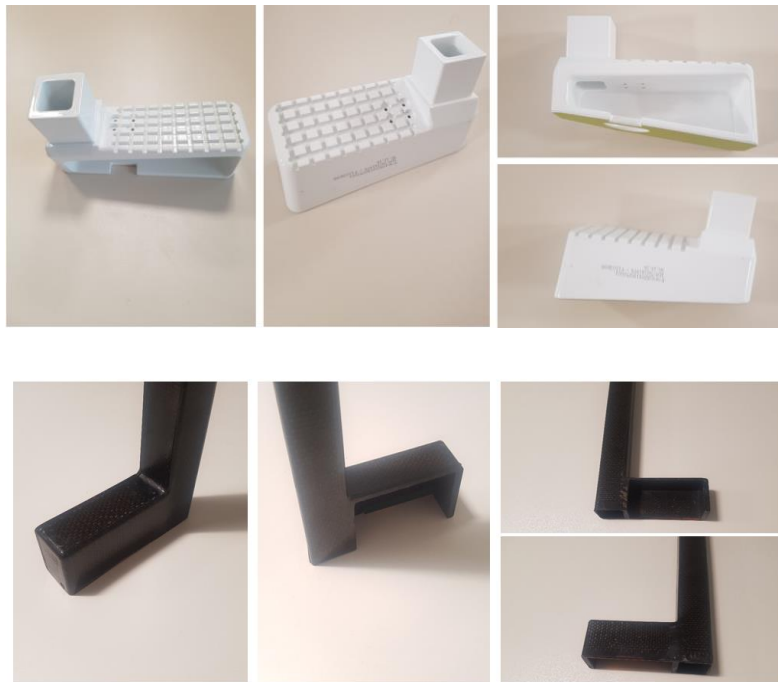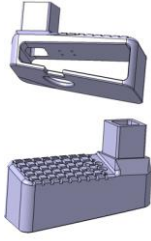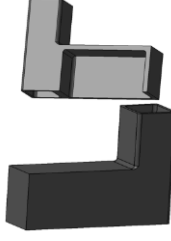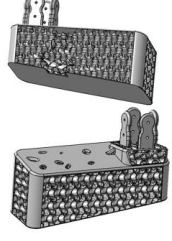
Figure 4.32. Detail views of existing designs

New lattice design is compared with existing conventional aluminum and single 3D woven resin molded design with respect to weight, material volume, maximum

displacement in load condition and safety factor. Safety factor for lattice design is kept the same as aluminum conventional design.

Table 4.5. Comparison of existing designs with new design

	Existing AL7050 Design	**Existing 3D-Woven Design**	**New Lattice Design**
Material	AL 7050 T7451	Composite	Ti-6Al-4V
Weight	449gr	249gr	243gr
Material Volume	158.663cm^3	215.397 cm^3	52.710 cm^3
Displacements	0.606mm	0.127mm	0.027mm
Reserve Factor	1.54	1.6	1.54

Figure 4.33. Material volume comparison with respect to design volume

The comparisons show that optimized new design with lattice structure has %46 lighter weight compared to conventional aluminum design and %3 lighter weight compared to 3D woven composite design while satisfying the same design requirements.

CHAPTER 5

CONCLUSION AND FUTURE WORK

This study is focused on implementation of gyroid lattice structures during topology optimization of an aircraft footstep. The performed study later on compared with previous studies.

Gyroid has a complex function driven shape that is created by many points in CAD platform. Related points, curves and surfaces that form the gyroid increases the size of the model data file. Two methods, beams and helixes, are used to lower the model data but neither works. Simplified gyroid geometry created by helixes/beams do not provide any performance improvement in digital modelling. Existing commercial computer technology does not satisfy the required computational technology for modelling larger components. Complex lattice structure geometry reduces the size of mesh in finite elements and in turn reduces loads on graphic card and memory during computation.

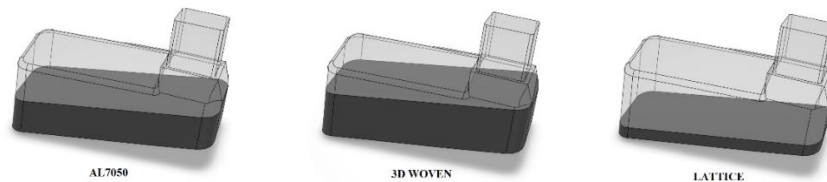Mock up builds show that most of the lattice geometries exist in literature need internal supports. The requirement of internal support limits the manufacturing orientation of the structural component. The manufacturing orientation limits the geometry of design due to overhang limitations.

SIMP optimization method can be implemented very quickly and simply for structural optimization. It has a huge potential for weight saving designs. It handles lattice geometries very well even the element size becomes smaller and it is totally geometry dependent.

Implementation of lattice structures into mechanical parts is an effective solution for weight reduction with the drawback of higher FEA computational time due to smaller element size. More complex and lighter shapes without any functionality loses can be

performed with topology optimization. Composite materials and conventional aluminum alloy designs can be outperformed with the additive manufacturing capabilities.

Topology optimization is performed for both materials, aluminum and titanium. The results show that aluminum component outperformed titanium component if there is no stress concentration point that do not allow geometry extension. Geometry extension provides higher order gain on stiffness. Higher volume with low-density component drives lighter designs when compared to lower volume and high-density components.

Lattice implementation extend the geometry dimensions to the maximum available design space without any weight penalty and it has significant positive effect on displacement of the component under the same load case with the same design space envelope.

During the optimization process, some parameters are kept constant to decrease complexity of the problem. Optimization envelope can be widen with the addition of following design parameters into optimization process as future work;

- Lattice thickness kept constant and only focused on residual volume during optimization process. Thickness and volume can be both taken into consideration as design parameters during optimization.
- Multiple lattice geometries can be implemented at the same time for a single component.
- Lattice geometry manipulation can be implemented in consideration of load distribution during optimization process.

Moreover, qualification of additive manufacturing process is needed for every component that is used in aerospace industry. Qualification of process is hard to perform for many companies due to high investment and labor costs. Qualification of aircraft components also can be taken as a future work for industrial applications.

REFERENCES

1- Haug, E.J. & Cea, J. (1981).*Optimization of Distributed Parameter Structures*. Netherlands. Sijjthoof&Noordoff,Alphen ann den Rijn.

2- S. Draper, B. Lerch, J. Telesman, R. Martin, I. Locci, A. Garg, A. Ring, (2016). *NASA/TM—2016-219136-Materials characterization of Electron Beam Melted Ti-6Al-4V*. NASA Glenn Research Center.

3- Yiğitbaşı, S.T. (2018).*Mechanical properties of Ti-6AL-4V parts produced by electron beam melting and topology optimization in different building directions*. Middle East Technical University. Ankara. Turkey

4- Badiru, A.B., Valencia, V.V. & Liu, D. (2017*). Additive Manufacturing Handbook: Product Development for the Defense Industry* (pp.271), CRC Press.

5- Daynes, S., Feih, S., Lu, W.F. & Wei, J. (2019). Design concepts for generating optimised lattice structures aligned with strain trajectories. *Computer Methods in Applied Mechanics and Engineering, 354*.

6- Li, D., Liao, W., Dai, N. & Xie, Y.M. (2020). Anisotropic design and optimization of conformal gradient lattice structures. *Computer-Aided Design, 119.*

7- Wu, J., Wang, C., Zhang, X. & Westermann, R. (2016). Self-Supporting Rhombic Infill Structures for Additive Manufacturing. *Computer-Aided Design, 80.* doi: 10.1016/j.cad.2016.07.006.

8- Clausen, A., Aage, N., & Sigmund, O. (2016). Exploiting Additive Manufacturing Infill in Topology Optimization for Improved Buckling. *Load,Engineering, 2(2)*.

9- Feng, J., Fu, J., Lin, Z., Shang, C., & Niu, X. (2019). Infill area generation from triply periodic minimal surfaces for additive manufacturing. *Computer-Aided Design, 107.*

10- Khaderi, S.N., Deshpande, V.S. & Fleck, N.A. (2014).The stiffness and strength of the gyroid lattice. *International Journal of Solids and Structures, 51(23–24)*

11- Isenberg, C. (1992). *The Science of Soap Films and Soap Bubbles*. New York: Dover,

12- Société Française des Mécaniciens, SFM. (1990) Afnor Technique, Guide de validation des prologiciels de calcul de structures(pp.124-125).

13- Röber, M. (2014). Multi objective topology optimization of truss structures for assembly devices using intelligent swarm techniques. *Procedia CIRP, 23*. doi:10.1016/j.procir.2014.10.083.

14- Podrouzek, J., Marcon, M., & Ninčević, K. & Wan-Wendner, R. (2019). Bio-Inspired 3D Infill Patterns for Additive Manufacturing and Structural Applications. Materials, 12, 499. doi:10.3390/ma12030499.

15- M. Zienkiewickz, Taylor R.L. (1989). *The finite element method* (4th edition, Vol. 1, pp.386). Butterworth-Heinemann

16- Burton, H., Eisenstein, N., Lawless, B., Jamshidi, P., Segarra, M., Addison, O., Shepherd, D., Attallah, M., Grover, L., & Cox, S. (2018). The design of additively manufactured lattices to increase the functionality of medical implants. *Materials science and engineering, 94.* doi:10.1016/j.msec.2018.10.052.

17- Schoen A. H. (1970).Infinite periodic minimal surfaces without self-intersections. NASA Technical Note TN D-5541.Infinite periodic minimal surfaces without self-intersections by Alan H. Schoen" (PDF). Archived (PDF) from the original on 2018-04-13. Retrieved 2019-04-12.

18- H. A. Schwarz. (1933). *Gesammelte mathematische abhandlungen*. Springer, Berlin,

19- Cheng, L., Bai, J., To, A. (2018). Functionally graded lattice structure topology optimization for the design of additive manufactured components with stress constraints. *Computer Methods in Applied Mechanics and Engineering, 344.* doi:10.1016/j.cma.2018.10.010.

20- Karcher, H. (1989). The triply periodic minimal surfaces of Alan Schoen and their constant mean curvature companions. M*anuscripta mathematica, 64 (3), 291–357.* doi:10.1007/BF01165824. ISSN 0025-2611.

21- Große-Brauckmann, K. & Meinhard, W. (1996). The gyroid is embedded and has constant mean curvature companions. *Calculus of Variations and Partial Differential Equations, 4(6), 499–523.* doi:10.1007/BF01261761. ISSN 0944-2669.

22- Shin, J., Kim, S., Jeong, D., Geun Lee, H., Lee, D., Lim, J. Y. & Kim, J. (2012). Finite element analysis of Schwarz-p surface pore geometries for tissue-engineered scaffolds. *Mathematical Problems in Engineering.* doi:10.1155/2012/694194.

23- Bennett, J.A., & Botkin, B. (1986). *The Optimum Shape:Automated Structral Design*. Plenum,New York.

24- Haug, E. J., Choi, K. K. & Komkov, V. (1986). *Design Sensivity Analysis for Discrte Structural Systems*.Academic,New York ,

25- Choi, K. & Seong, H. (1986). A Numerical Method for Shape Design Sensitivity Analysis and Optimization of Built-up Structures. doi:10.1007/978-1-4615-9483-3_13.

26- Prager, W., Rozvany, G. I. N. (1977) *Optimization of Structural geometry,in Dynamical Systems* (eds.A.R.Bednarek , L.Cesari).Qacademic Press, New York

27- Rozvany, G. I. N. (1981) Optimality criteria for grids,shells and arches. *Optimization of distributed parameter structures*. Netherlands. Sijjthoof&Noordoff,Alphen ann den Rijn

28- Michell, A.G.M. (1904). The limits of economy of material in frame structures.*Philosophical Magazine, 8,589-97*

29- Hemp, W. S.(1973) *Optimum Structures*. Clarendon, Oxford.

30- Lagache, J. M. (1981) , Developments in Michell theory. *International Symposium on Optimal Structure* Design.Tuscon ,

31- Liu J. & Ma Y. (2016) A survey of manufacturing oriented topology optimization methods. *In Advances in Engineering Software*, *100*, 161-175.

32- Bogue, R. (2013). 3-D printing: The dawn of a new era. *Manufacturing Assembly Automation, 33*(4), 307—311.

33- Berman, B. (2012). 3-D printing: The new industrial revolution. *Business Horizons, 55*(2), 155—162.

34- Wohlers Associates Inc. (2013). *Wohlers report*. Fort Collins, CO: Wohlers.

35- Powder Bed Fusion: Additive Manufacturing Research Group: Loughborough University (2019), Retrieved from https://www.lboro.ac.uk/research/amrg/about/the7categoriesofadditivemanufacturing/powderbedfusion/

36- A case study on topology optimized design for additive manufacturing: https://www.researchgate.net/figure/Comparative-illustration-of-size-shape-and-topology-optimization-Structural_fig1_321771366 [accessed 8 Dec, 2019]

37- Bendsøe, M. P. & Kikuchi, N. (1988). Generating optimal topologies in structural design using a homogenization method. *Computer Methods in Applied Mechanics and Engineering, 71*, 2.

38- Bendsøe, M. (1989). Optimal Shape Design as a Material Distribution Problem. *Structural Optimization, 1,* 193-202. doi:10.1007/BF01650949.

39- Zhou M. & Rozvany G. I. N. (1991) The COC algorithm, part II: topological, geometry and generalized shape optimization. *Computing Methods Applied Mechanical Eng., 89*(1–3),309–336

40- Mlejnek H.P. (1992). Some aspects of the genesis of structures. *Structural Optimization 5,* 64–69.

41- Stolpe M., Svanberg K. (2001). On the trajectories of penalization methods for topology optimization. *Structural multidisciplinary Optimization,21,*128–139

42- Eschenauer H. A., Kobelev V. V. & Schumacher A. (1994). Bubble method for topology and shape optimization of structures. *Structural Optim 8*:42-51

43- Bourdin B. & Chambolle A. (2003). Design-dependent loads in topology optimization. *ESAIM Control Optim Calc Var 9,*19–48

44- Wang, M. & Zhou, S. (2004). Phase field: A variational method for structural topology optimization. *CMES. Computer Modeling in Engineering & Sciences, 6.*

45- Kennedy, J. & Eberhart, R. (1995). Particle Swarm Optimization. IEEE *International Conference on Neural Networks. IV*, 1942–1948.

46- Khandelwal, K. & Tovar, A. (2010). Hybrid Cellular Automaton: A Novel Framework for Non-Linear Topology Optimization. *19th Analysis and Computation Specialty Conference*. doi:10.1061/41131(370)37.

47- Svanberg, K. (1987). The method of moving asymptotes a new method for structural optimization. *International Numerical Methods Eng., 24,*359–373

48- Svanberg, K. (2002). A class of globally convergent optimization methods based on conservative convex separable approximations. *SIAM Journal on Optimization, 12*(2):555–573. doi:10.1137/S1052623499362822

49- Eschenauer, H., Olhoff, N. & Schnell W. (1997). *Applied structural mechanics* (pp. 42). H. Springer

50- Martin, H. S. (2009). *Elasticity, Theory, applications and numeric (*pp. 122). Elsevier.

51- Bendsoe, M. P. & Sigmund, O. (2003). *Topology Optimization, Theory Methods and applications* (pp. 1-47). Springer Verlag ISBN 3-540-48992-1.

52- Dierkes, U., Hildebrandt, S., Küster, A., Wohlrab, O. (1992). Minimal Surfaces I. *Grundlehren der mathematischen wissenschaften, 295. Springer, Berlin*

53- Lagrange, J. L. (1760). Essai d'une nouvelle methode pour determiner les maxima et les minima des formules integrales indefinies. *Miscellanea Taurinensia 325*

APPENDIX A

BASIC MATLAB CODE FOR CANTILEVER BEAM PROBLEM

Matlab code for topology optimization using a reaction diffusion equation

```
function [str,phi] = Cantileverbeam(numelx,numely,v_max,tau_x)
%% Parameter definition
E0 = 1;
e_min = 1e-4;
N_u = 0.3;
nvol = 100;
dt = 0.1;
d = -0.02;
p = 4;
phi = ones((numely+1)*(numelx+1),1);
str = ones(numely,numelx);
volInit = sum(str(:))/(numelx*numely);
%% Finite element analysis preparation
% For displacement field
A11 = [12 3 -6 -3; 3 12 3 0; -6 3 12 -3; -3 0 -3 12];
A12 = [-6 -3 0 3; -3 -6 -3 -6; 0 -3 -6 3; 3 -6 3 -6];
B11 = [-4 3 -2 9; 3 -4 -9 4; -2 -9 -4 -3; 9 4 -3 -4];
B12 = [ 2 -3 4 -9; -3 2 9 -2; 4 9 2 3; -9 -2 3 2];
KE = 1/(1-N_u^2)/24*([A11 A12;A12' A11]+N_u*[B11 B12;B12' B11]);
% For Topological derivative
a1 = 3*(1-N_u)/(2*(1+N_u)*(7-5*N_u))*(-(1-14*N_u+15*N_u^2)*E0)/(1-2*N_u)^2;
a2 = 3*(1-N_u)/(2*(1+N_u)*(7-5*N_u))*5*E0;
A = (a1+2*a2)/24*([A11 A12;A12' A11]+(a1/(a1+2*a2))*[B11 B12;B12' B11]);
nodenrs = reshape(1:(1+numelx)*(1+numely),1+numely,1+numelx);
Edof_v = reshape(2*nodenrs(1:end-1,1:end-1)+1,numelx*numely,1);
edofMat = repmat(Edof_v,1,8)+repmat([0 1 2*numely+[2 3 0 1] -2 -1],numelx*numely,1);
iK = reshape(kron(edofMat,ones(8,1))',64*numelx*numely,1);
jK = reshape(kron(edofMat,ones(1,8))',64*numelx*numely,1);
% For Reaction diffusion equation
NNdif_e = 1/6*[ 4 -1 -2 -1;-1 4 -1 -2;-2 -1 4 -1;-1 -2 -1 4];
```

```matlab
NN_e = 1/36*[ 4 2 1 2;2 4 2 1;1 2 4 2;2 1 2 4];

edofVec2= reshape(nodenrs(1:end-1,1:end-1)+1,numelx*numely,1);

edofMat2= repmat(edofVec2,1,4)+repmat([0 numely+1 numely -1],numelx*numely,1);

iN = reshape(kron(edofMat2,ones(4,1))',16*numelx*numely,1);

jN = reshape(kron(edofMat2,ones(1,4))',16*numelx*numely,1);

sNN = reshape(NN_e(:)*ones(1,numely*numelx),16*numelx*numely,1);

NN = sparse(iN,jN,sNN);

sNNdif = reshape(NNdif_e(:)*ones(1,numely*numelx),16*numelx*numely,1);

NNdif = sparse(iN,jN,sNNdif);

%% Loads and boundary settings

F = sparse(2*(numely+1)*(numelx+1),1);

U = zeros(2*(numely+1)*(numelx+1),1);

F((numely+1)*(numelx)*2+numely+2*(-
round(numely/32)+1):2:(numely+1)*(numelx)*2+numely+2*(round(numely/32)+1),1) = 1;

fixeddofs = 1:2*(numely+1);

alldofs = 1:2*(numely+1)*(numelx+1);

freedofs = setdiff(alldofs,fixeddofs);

T = NN/dt + tau_x*(numely*numelx)*NNdif;

fixeddofs_phi = sort([1:numely+1 numely+2:numely+1:(numely+1)*(numelx) 2*(numely+1):numely+1:(numely+1)*(numelx)
...

(numely+1)*numelx+1:(numely+1)*(numelx+1)]);

phi(fixeddofs_phi) = 0;

alldofs_phi = 1:(numely+1)*(numelx+1);

freedofs_phi = setdiff(alldofs_phi,fixeddofs_phi);

%% Main loop

for iterNum = 1:200

    % FE-analysis, calculate sensitivities

    sK = reshape(KE(:)*(e_min+str(:)'*(E0-e_min)),64*numelx*numely,1);

    K = sparse(iK,jK,sK);

    K = (K+K')/2;

    U(freedofs) = K(freedofs,freedofs) \ F(freedofs);

    SED = (e_min+str*(E0-e_min)).*reshape(sum((U(edofMat)*KE).*U(edofMat),2),numely,numelx);

    TD = (1e-4+str*(1-1e-4)).*reshape(sum((U(edofMat)*A).*U(edofMat),2),numely,numelx);

    td2=[TD(1,1) TD(1,:) TD(1,end); TD(:,1) TD TD(:,end) ; TD(end,1) TD(end,:) TD(end,end)];

    TDN = 0.25*(td2(1:end-1,1:end-1)+td2(2:end,1:end-1)+td2(1:end-1,2:end)+td2(2:end,2:end));

    objective(iterNum) = sum(SED(:));

    vol = sum(str(:))/(numelx*numely);
```

```matlab
% Print results
disp(['It.: ' num2str(iterNum) ' Compl.: ' sprintf('%10.4e',objective(iterNum)/((numelx*numely)))...
    ' Vol.: ' sprintf('%6.2f',vol)])
colormap(gray); imagesc(-str,[-1,0]); axis equal; axis tight; axis off; drawnow;
% Check for convergence
if iterNum>nvol && (abs(vol-v_max)<0.005) && all(abs(objective(end)- ...
        objective(end-5:end-1))< 0.01*abs(objective(end)))
    return;
end
% Set augmented Lagrangian parameters
ex = v_max+(volInit-v_max)*max(0,1-iterNum/nvol);
lambda = sum(sum(TDN))/((numely+1)*(numelx+1))*exp(p*((vol-ex)/ex+d));
C = 1/sum(abs(TDN(:)))*(numely*numelx);
g2 = reshape(TDN,(numely+1)*(numelx+1),1);
% Update level set function
Y = NN*(C*(g2-lambda*ones(size(g2)))+phi/dt);
phi(freedofs_phi,:) = T(freedofs_phi,freedofs_phi) \ Y(freedofs_phi,:);
phi = min(1,max(-1,phi));
phin = reshape(phi,numely+1,numelx+1);
phie = 0.25*(phin(1:end-1,1:end-1)+phin(2:end,1:end-1)+phin(1:end-1,2:end)+phin(2:end,2:end));
str(:,:) = (phie(:,:)>0);
end
```

APPENDIX B

BASIC MATLAB CODE FOR GYROID

```
[y,x,z] = ndgrid(linspace(0,20),linspace(0,20),linspace(0,20));
cx = cos(x);
cy = cos(y);
cz = cos(z);
sx = sin(x);
sy = sin(y);
sz = sin(z);
f = cx.*sy+cy.*sz+cz.*sx;
cla
isosurface(x,y,z,f);
view(3);
camlight axis equal
```